EFFECTS OF PRIOR STIMULATION ON TACTILE EVOKED EPIDURAL FIELD POTENTIALS IN RAT S1 CORTEX

by

ASLI AKDENİZ KARATAY

M.D., in Medicine, Istanbul University Cerrahpaşa Faculty Of Medicine, 2019

Submitted to the Institute of Biomedical Engineering
in partial fulfillment of the requirements
for the degree of
Master of Science
in
Biomedical Engineering

Boğaziçi University
2023

ACKNOWLEDGMENTS

I would like to start by expressing profound gratitude to my supervisor, Prof. Dr. Burak Güçlü. His patience, dedicated time, and meticulous mentorship throughout my master's thesis journey have been invaluable.

I would like to thank Begüm Devlet Kılıçkap and Deniz Kılınç Bülbül for their continuous support during my experimental work.

I am grateful for the support of my life partner, Onurhan Karatay. His patience has been my source of motivation, offering me strength to persist whenever I stumbled.

Lastly, I would like to express my gratitude to my beloved family: my mother, Gülçin Akdeniz, my father, Vefa Asım Akdeniz, and my sister, Eda Akdeniz. Their unyielding faith in my decisions, unwavering support regardless of the circumstances, and understanding, even when my choices deviated from the norm, have allowed me to discover myself. This thesis is dedicated to them.

This work was supported by TÜBİTAK grant no:117F481 under European Union's FLAG-ERA JTC 2107 project GRAFIN and H2020 Graphene Flagship Core 2.

ACADEMIC ETHICS AND INTEGRITY STATEMENT

I, Aslı Akdeniz Karatay, hereby certify that I am aware of the Academic Ethics and Integrity Policy issued by the Council of Higher Education (YÖK), and I fully acknowledge all the consequences due to its violation by plagiarism or any other way.

Name :

Signature:

Date:

ABSTRACT

EFFECTS OF PRIOR STIMULATION ON TACTILE EVOKED EPIDURAL FIELD POTENTIALS IN RAT S1 CORTEX

Understanding how tactile sensation is processed in the somatosensory cortex is crucial for the development of neuroprostheses that can provide a realistic sense of touch. Exploring the electrophysiological basis of vibrotactile forward masking offers valuable insights into how the brain integrates and responds to sequential sensory inputs. This understanding can help drive progress in the development of haptic interfaces and the enhancement of neuroprosthetic technologies designed to improve tactile perception. Epidural field potentials were recorded from the hind paw representation of the rat S1 cortex by using various experimental parameters. The effects of the prior stimulus on the test stimulus window measured as dB difference and latency difference were evaluated. The results indicated that all main factors had a significant impact on the dB difference. An increase in the amplitude of the prior stimulus was found to enhance suppression effects. The suppression decreased as the temporal gap increased. By demonstrating the impact of the prior stimulus, the study underscores the fundamental influence of preceding sensory inputs in shaping subsequent sensory processing.

Keywords: Primary Somatosensory Cortex, Epidural Field Potentials, Forward Masking, Neuroprosthetics

ÖZET

ÖN UYARIMIN SIÇAN S1 KORTEKSİNDE ÖLÇÜLEN TAKTİL UYARILMIŞ EPİDURAL ALAN POTANSİYELLERİNE ETKİSİ

Dokunma duyusunun somatosensoriyel kortekste nasıl işlendiğini anlamak, gerçekçi bir dokunma duyusu sağlayabilen nöroprotezlerin geliştirilmesi için çok önemlidir. Ayrıca vibrotaktil ileri maskelemenin elektrofizyolojik temelini anlamak, beynin sıralı duyusal girdileri nasıl birleştirdiğine ve bunlara nasıl yanıt verdiğine dair değerli bilgiler sunar. Bu tezde sıçan S1 korteksinin arka ayak bölgesinden epidural alan potansiyelleri ölçülerek çeşitli taktil parametrelerin (frekans, genlik, iki uyaran arası süre) etkisine bakıldı. Özellikle ardışıl gelen iki uyarandan ilkinin ikincisinin yarattığı potansiyellere etkisi genlik ve latans farkları olarak değerlendirildi. Sonuçlar tüm ana faktörlerin genlik farkı üzerinde istatistiksel anlamlı bir etkiye sahip olduğunu göstermiştir. Örneğin ilk uyaranın genliğindeki artış ikinci uyarana verilen cevabı baskılamıştır. Ancak bu baskılama iki uyaran arasındaki süre arttıkça azalmıştır. Bu sonuçlar hem temel bilimsel açıdan, hem de nöroprotezlerin ve haptik arayüzlerin geliştirilmesi için ardışıl vibrotaktil uyaranların duyusal işlemeyi şekillendirmekteki önemini vurgulamaktadır.

Anahtar Sözcükler: Birincil Somatosensoriyel Korteks, Epidural Alan Potansiyelleri, İleri Maskeleme, Nöroprotezler

TABLE OF CONTENTS

ACKNOWLEDGMENTS iii
ACADEMIC ETHICS AND INTEGRITY STATEMENT iv
ABSTRACT v
ÖZET vi
LIST OF FIGURES ix
LIST OF TABLES xiv
LIST OF SYMBOLS xv
LIST OF ABBREVIATIONS xvi
1. INTRODUCTION 1
1.1 Motivation and Objectives 1
1.2 Outline 4
2. BACKGROUND 5
2.1 Somatosensory System & Sensation of Touch 5
2.1.1 Physiological Properties of Glabrous Skin Mechanoreceptors . . 7
2.1.2 Rat Primary Somatosensory Cortex 10
2.2 Recording Electrical Activity of the Brain 16
2.2.1 EEG 18
2.2.2 ECoG 20
2.2.3 Local Field Potentials 22
2.2.4 Action Potentials 24
2.3 Psychophysical Methods for Measurement of Sensation 26
2.3.1 Four-Channel Model in Tactile Psychophysics 28
2.3.2 Masking 29
3. METHODOLOGY 33
3.1 Subjects 33
3.2 Apparatus 34
3.3 Surgery 35
3.4 Vibrotactile Stimuli and Epidural Field Potentials 37
3.5 Procedure 39

3.6 Data Analysis 40
4. RESULTS 45
4.1 Qualitative Description of the Recorded Traces 45
4.2 Tactile Evoked Epidural Field Potentials 48
4.2.1 Epidural Field Potential Amplitude Changes Due to Prior Stimulation 49
4.2.2 Epidural Field Potential Latency Changes Due to Prior Stimulation 56
5. DISCUSSION 63
5.1 Overall Conclusion 63
5.2 Comparison with the Previous Literature 64
5.3 Limitations and Future Work 66
REFERENCES 68

LIST OF FIGURES

Figure 2.1 The somatosensory pathway is illustrated by the transmission of afferent peripheral fibers, muscle spindles, Golgi tendon organs, and receptors located in the joints and skin are shown. The fibers transmit this information to the spinal cord, where they split into intra-segmental and supra-segmental projections that communicate with neurons in the dorsal horn and brainstem. In the thalamus, neurons synapse, and projections terminate in the postcentral gyrus within the somatosensory cortex. Reproduced from [1]. 6

Figure 2.2 Mechanoreceptors are presented in hairless skin. The top row indicates the location of mechanoreceptors within the dermal structure, while the bottom row provides information about the area covered by their receptive fields (spatial scope). The neural firing pattern of these receptors upon receiving a ramp and hold stimulus is also depicted. Reproduced from [1]. 8

Figure 2.3 The relationship between the mean firing rate and the intensity of stimulation in a cat's rapidly adapting (RA) fiber is depicted. Plots show intensity characteristic parameters (a0-a3) of a cat RA fiber at two different frequencies, at 20 Hz and 50 Hz, respectively.(Adopted from Güçlü and Bolanowski, 2003 [2]. 11

Figure 2.4 Spike histograms are depicted. The stimulus waveform is shown above the PSTHs; black bars correspond to the condition of the sham, while white bars represent the bicuculline application.(Reproduced from Vardar and Güçlü, 2017 [3]. 15

Figure 2.5 Various methods are used to quantify the brain's electrical activity are shown. (a) Depicts different scales such as EEG (A), ECoG (B), and single/multi-unit recordings (C) Reproduced from [4]. (b) Shows the part of recorded electrical signals. Modified from [5]. 17

Figure 2.6 Simultaneous recording was conducted using a subdural grid array consisting of three electrodes positioned over the left temporal cortex and using a strip that has 8 contacts placed on the surface of the left hemisphere (recording ECoG signals), and in a patient with epilepsy, scalp electroencephalography (EEG) was performed over both hemispheres (fz and O2). Compared to scalp EEG, ECoG signals are larger in amplitude and have a greater resolution at higher frequencies. Modified from [6]. 21

Figure 2.7 Tuning characteristics of spikes while subjects control the neural cursor. (a) A raster plot showing spiking patterns of 33 units recorded simultaneously while performing neural cursor point-and-click and the Radial-8 tasks on Day 1000. The trial began at time 0 (indicated by the left perpendicular line) and ended at 6.18 s (indicated by the right perpendicular line). (b) Spike activity of a neuron while the subject does the Radial-8 task. For each of the eight directions of movement, a tick represents the spike activity, and a movement is depicted by each row of ticks. Histograms show spiking activity across trials. c) The top row displays the tuning of all the neurons in relation to the direction of the movement; the radius of the circle corresponds to a modulation depth of 1. The bottom row depicts the unit counts tuned significantly in eight different cardinal task directions, presented within 45-degree bins. Reproduced from [7]. 27

Figure 2.8 Illustration of backward, forward, and simultaneous masking. Reproduced from [8]. 29

Figure 2.9 Mean threshold shifts are depicted as a function of masking stimulus duration; the x-axis represents the duration of the masking stimulus in ms. (a) illustrates the shifts in thresholds obtained with 250 Hz stimulation, where the amount of masking significantly increased with increasing duration and amplitude of the masking stimulus ($p < 0.001$, $p < 0.01$), respectively. (b) Similar functions were obtained for the 20 Hz stimulation, where the amount of masking increased with both the duration and the level of the masking stimulus ($p < 0.0001$). Reproduced from Gescheider et al., 1995 [9]. 31

Figure 3.1 Distributions of subjects are shown. (a) represents the age distribution, and (b)represents the weight distribution. 33

Figure 3.2 The diagram of the experimental setup is depicted. Modified from [10]. 34

Figure 3.3 Illustration of the craniotomy window targeting the hind paw representation of the somatosensory cortex and the electrode placed on the dura mater. (a) The functional atlas of the rat somatosensory cortex indicates the craniotomy window, demarcated by the red lines, and the approximate hind paw representation, represented by the red cross. Modified from [11]. (b) Placement of the electrode over duramater. 36

Figure 3.4 The waveforms used for mechanical stimulation. The first row shows the 5 Hz (a), 40 Hz (b), and 250 Hz (c) test stimuli, respectively. An example of experimental conditions with a 100 msec temporal gap is depicted on the 2nd row (d, e, f) and 300 msec on the 3rd row (g, h, i). Note that, in some experimental conditions, the frequencies of the prior and test stimuli were different, not shown in this figure. 39

Figure 3.5 Anaysis windows are depicted. Traces are baseline shifted for plotting purposes. Tb: Baseline, To: Onset period. 41

Figure 4.1 Plots from trial by trial analysis of Tactile Evoked Potentials from experiment 220408. The variation in colors denotes different conditions representing different amplitude levels for each frequency pair; the first row of each figure represents the conditions where only the test stimulus was presented with the highest amplitude. The next four rows (3-6) represent the conditions where the prior and test stimuli were presented, with varying amplitude levels for each. Traces recorded from Ch-1 for (a) 5-5 Hz with a 100 msec temporal gap, (b) 250-250 Hz with a 300 msec temporal gap. 46

Figure 4.2 Time-averaged Epidural Field potentials were plotted from experiment 220408. Only experiments with prior and test stimulus pairs having the same frequency value were plotted. In (a), (c), and (e) the temporal gap is 100 milliseconds between the stimulus pairs, while in (b), (d), and (f) the temporal gap is 300 milliseconds between stimuli. 48

Figure 4.3 The effect of the temporal gap on the dB difference. The results are shown for a 5 Hz prior stimulus frequency and test stimulus frequencies of 5 Hz (a), 40 Hz (b), and 250 Hz (c), with temporal gaps of 100 msec and 300 msec (color code: light blue for 100 msec and dark blue for 300 msec). The standard error of the mean (SEM) is shown by error bars. 50

Figure 4.4 The results are shown for a 40 Hz prior stimulus frequency and test stimulus frequencies of 5 Hz (a), 40 Hz (b), and 250 Hz (c), with temporal gaps of 100 msec and 300 msec (color code: light blue for 100 msec and dark blue for 300 msec). 51

Figure 4.5 The results are shown for a 250 Hz prior stimulus frequency and test stimulus frequencies of 5 Hz (a), 40 Hz (b), and 250 Hz (c), with temporal gaps of 100 msec and 300 msec (color code: light blue for 100 msec and dark blue for 300 msec). 52

Figure 4.6 The effect of the prior stimulus on the latency difference. The results are shown for a 5 Hz prior stimulus frequency and test stimulus frequencies of 5 Hz (a), 40 Hz (b), and 250 Hz (c), with temporal gaps of 100 msec and 300 msec (color code: light blue for 100 msec and dark blue for 300 msec). The standard error of the mean (SEM) is shown by error bars. 57

Figure 4.7 The effect of the prior stimulus on the latency difference. The results are shown for a 40 Hz prior stimulus frequency and test stimulus frequencies of 5 Hz (a), 40 Hz (b), and 250 Hz (c), with temporal gaps of 100 msec and 300 msec (color code: light blue for 100 msec and dark blue for 300 msec). The standard error of the mean (SEM) is shown by error bars. 58

Figure 4.8 The effect of the prior stimulus on the latency difference. The results are shown for a 250 Hz prior stimulus frequency and test stimulus frequencies of 5 Hz (a), 40 Hz (b), and 250 Hz (c), with temporal gaps of 100 msec and 300 msec (color code: light blue for 100 msec and dark blue for 300 msec). The standard error of the mean (SEM) is shown by error bars. 59

LIST OF TABLES

Table 3.1	Conversion table of the corresponding attenuation values to vibrotactile displacement amplitudes (zero to peak).	38
Table 4.1	Mean dB difference and standard error of conditions for each frequency pair found by the linear mixed-effects model.	54
Table 4.2	mean and standard error of the interaction between frequency and amplitude of the test stimulus.	55
Table 4.3	The mean and standard error of the interaction between amplitude and frequency of the prior stimulus and temporal gap.	55
Table 4.4	Effect of each frequency pair on latency difference found by the linear mixed-effects model.	61
Table 4.5	Effect of the interaction between the prior stimulus' frequency and test stimulus' amplitude on latency difference.	61

LIST OF SYMBOLS

$A_{peak-to-peak}$	Peak-to-peak Amplitude
V_{RMS}	Root-mean-square of the Voltage

LIST OF ABBREVIATIONS

AP	Action Potential
BMI	Brain-Machine Interface
CNS	Central Nervous System
DRG	Dorsal Root Ganglia
EEG	Electroencephalography
ECoG	Electrocorticography
EFP	Epidural Field Potential
ERPs	Event-Related Potentials
FAI	Fastly Adapting
ISI	Interstimulus Interval
LFP	Local Field Potential
MEG	Magnetoencephalogram
PC	Pacinian Corpuscle
PNS	Peripheral Nervous System
PMBSF	Posterior-medial Barrel Sub-field
RA1	Rapidly Adapting Type 1
RA2	Rapidly Adapting Type 2
RF	Receptive Field
SAI	Slowly Adapting I
SAII	Slowly Adapting II
SI	Primary Somatosensory Cortex
SNR	Signal-to-Noise Ratio
SBR	Signal-to-Baseline Ratio

1. INTRODUCTION

1.1 Motivation and Objectives

In everyday life, we receive sensory stimuli sequentially, one after another. This sequential presentation of sensory stimuli allows the brain to integrate and process information from the same and different sensory organs –in a meaningful way to create a coherent perception of the world. A sequential presentation of sensory stimuli can help the brain integrate information by using the temporal order of the stimuli. For instance, sensory stimuli may co-occur or occur within close temporal proximity, which can create challenges for the brain, as it must sort out and integrate the different sensory inputs in a way that makes sense.

Masking is one example of how the presence of one sensory stimulus can impact the perception of another stimulus by modifying or inhibiting its processing, highlighting the complex nature of sensory processing in the brain. Sensory adaptation processes have advantages and disadvantages in perception. These processes, such as masking, emphasize specific differences between stimuli, allowing for selective attention and filtering out irrelevant information. However, a significant disadvantage of sensory adaptation is decreased sensitivity and duration of action, which results from a rapid decline in neuronal activity over time, leading to difficulty detecting or discriminating in consecutive stimuli, mainly when they occur in close temporal proximity.

Masking has been observed across various sensory modalities, including visual, auditory, olfactory, and tactile. Masking in vision occurs when a visual stimulus is made difficult to perceive or utterly invisible due to the presence of another stimulus. For instance, in the visual domain, a well-known form of masking is the phenomenon called meta-contrast masking, where a briefly presented target stimulus is followed immediately by a masking stimulus, making the target more difficult to perceive. In the auditory domain, a classic example of masking is simultaneous masking. In this

case, a signal tone is made less audible by simultaneously presenting a masking noise (e.g., white noise or a tone at a different frequency). Masking in the tactile domain occurs when one tactile stimulus interferes with the detection or perception of another tactile stimulus. A brief tactile stimulus presented to one part of the skin can make it more difficult to detect or perceive a subsequent tactile stimulus presented to the same or a different part of the skin.

Sensory perception studies commonly employ a range of masking techniques, utilizing various types of stimuli. A forward masking stimulus occurs before the test stimulus; a backward masking stimulus occurs after the test stimulus, or a simultaneous masking stimulus starts and ends simultaneously with the masking stimulus. Each of these techniques can be used to investigate different aspects of sensory perception and the neural mechanisms underlying perception and attention.

Tactile masking has been observed across various sensory tasks, including detection, discrimination, and localization, and has been studied extensively in both humans and animals. Several stimulus parameters influence the amount of masking: amplitude, frequency, the duration of the test stimulus, the duration of the masking stimulus, and the temporal gap between stimuli (interstimulus interval, i.e., ISI). The literature suggests that various factors can influence the amount of masking. Studies have reported that increasing the length of the ISI and the test stimulus duration can decrease masking while decreasing the length of ISI and the magnitude of the masking stimulus can have the opposite effect. The effectiveness of masking greatly relies on the alignment between the test and masking stimuli, as well as the presence of a masking site on the skin, which plays a crucial role.

Investigating how the brain processes and integrates sensory information has substantial implications for designing devices that emulate natural tactile sensations and offer users realistic feedback. This holds particular relevance in developing neuroprostheses that aim to restore the sense of touch in individuals who have lost their ability for various reasons. This effort should also include a focused investigation into intricate phenomena such as masking, as understanding the physiological mechanisms

of masking will be crucial in developing technologies for haptic interfaces since they need to provide realistic tactile feedback to users to foster a feeling of complete immersion and a heightened sense of presence within the virtual environment.

Our goal is to understand the neural underpinnings of consecutive tactile stimulation in a rat model and address the existing gap in the literature regarding the electrophysiological relevance of vibrotactile forward masking mechanisms. Tactile-evoked epidural field potentials were recorded using multichannel surface electrodes (micro-ECoG) from the rat SI cortex's (Primary Somatosensory cortex) hind paw representation. Specifically, we aimed to understand how prior stimulation affects the neural response elicited by subsequent stimulation within the time window of the latter stimulation. Our hypothesis posits that the neural response evoked by the prior stimulation exerts suppressive effects on the subsequent stimulation. We anticipate that the magnitude of suppression will be influenced by the frequency and amplitude of both stimuli, with increased suppression occurring when stimuli are presented at the same frequency and in closer temporal proximity. Moreover, an increase in the amplitude of the prior stimulus is expected to increase the degree of suppression. Conversely, we predict an inverse relationship between the amplitude of the test stimulus and the extent of suppression. To test these hypotheses, we employed an experimental paradigm involving various frequency and amplitude levels for the first and second stimuli and different temporal gaps as a variable and measured latency and peak-to-peak values.

The thesis introduces a novel approach by analyzing epidural field potentials through consecutive vibrotactile stimulation. Advancing our understanding of sensory encoding mechanisms is beneficial for enhancing high-quality Brain-Machine Interfaces (BMIs) that rely on sensory feedback.

1.2 Outline

The thesis follows the following structure: Chapter 2 provides background information about the somatosensory system, recording methods of brain signals, and psychophysical methods. Chapter 3 outlines the experimental procedures. Chapter 4 presents the results, while Chapter 5 offers their interpretations.

2. BACKGROUND

2.1 Somatosensory System & Sensation of Touch

Sensory information, in its most basic form, refers to the neural activation produced by specialized cells in the body, known as receptor cells, in response to various types of stimuli. The neural information is translated starting from the peripheral nervous system (PNS) to the central nervous system (CNS) through a combination of serial and parallel neural connections. During this transmission, the information passes through a network of neurons and synapses, in which existing signals are added to the new ones and summed up. As a result, the brain can integrate multiple sensory information sources to create a complete understanding of the environment.

Upon being exposed to a stimulus, a sensory receptor triggers a series of chemical reactions that lead to electrical signals known as action potentials. Specifically, the somatosensory pathway transmits sensory information related to touch, pain, temperature, and proprioception from the periphery to the cortex. The somatosensory pathway has three classifications of neurons located in the dorsal root ganglia (DRG), spinal cord, and thalamus. The first-order neuron has a peripheral axon that terminates at specialized sensory receptors with distinct morphological characteristics and is located in different body parts, enabling specificity and discrimination among various somatosensation types, including proprioception, exteroception, and interoception. The nuclei of first-order neurons are located in the DRG. The DRG is a collection of sensory neuron cell bodies located near the spinal cord and develops from neural crest cells originating from the edges of the neural tube during embryonic development [12]. Due to its derivation from neural crest cells instead of the neural tube, the DRG can be considered as the spinal cord's gray matter that travels to the outer regions or periphery. The survival and the transformation of neural crest cells into DRG components depend on an early signal from CNS. This signal needs to be provided within the first few hours after the initiation of migration to ensure optimal neural crest cell differenti-

ation and survival. Throughout the phases of embryonic development, the DRG axons are grouped together to form 31 spinal nerves, which correspond to specific regions of the body that they innervate. Each has a sensory and motor division, thus forming the peripheral nerves [1].

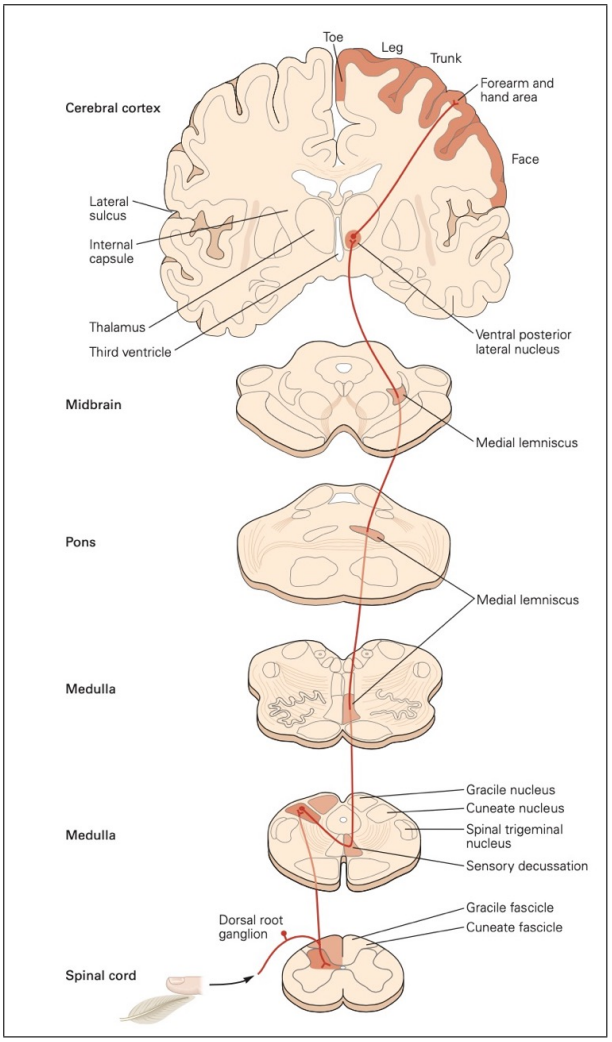

Figure 2.1 The somatosensory pathway is illustrated by the transmission of afferent peripheral fibers, muscle spindles, Golgi tendon organs, and receptors located in the joints and skin are shown. The fibers transmit this information to the spinal cord, where they split into intra-segmental and supra-segmental projections that communicate with neurons in the dorsal horn and brainstem. In the thalamus, neurons synapse, and projections terminate in the postcentral gyrus within the somatosensory cortex. Reproduced from [1].

The dermatome encompasses both the superficial skin and the underlying tissues, receiving sensory innervation from designated peripheral nerves. The primary somatosensory cortex (SI) receives projections from these peripheral nerves. SI exhibits a somatotopic organization, where specific cortex regions correspond to specific

bodily elements, reflecting the cortical representation of each anatomical area. The DRG neuron's central branch projects into the spinal cord's dorsal horn. They ascend ipsilaterally through fasciculus cuneatus and synapse with second-order neurons in the medulla oblongata. The crossing of axons of second-order neurons forms sensory decussation in the medulla, as shown in Figure 1. These fibers ascend and establish synaptic connections with neurons within the VPN, and after they synapse, they terminate in the postcentral gyrus in S1.

Within the somatosensory system, there are different types of receptors for sensing different modalities; thermoreceptors detect object temperature; while nociceptors perceive stimuli such as pain, and itch receptors react to stimuli that cause itching. Mechanoreceptors are sensory receptors that convert mechanical stimuli, such as pressure and vibration, into receptor potentials. The sense of touch is produced by distinct types of mechanoreceptors that detect various forms of skin distortion, motion, and vibration. Within the muscles, three different types of mechanoreceptors send signals regarding the length of the muscle, motion velocity, and force, whereas mechanoreceptors located in the joint capsule are responsible for signaling joint angle.

2.1.1 Physiological Properties of Glabrous Skin Mechanoreceptors

Millions of particular sensory receptors in the human body contribute to the richness of sensory experience. Often, a specific kind of energy will stimulate a selective receptor at a specific location on the body and only respond to energy with a particular pattern of temporal or spatial dimensions. Each sensory system establishes a common signaling mechanism when the receptor converts the energy of sensory stimulation into common electrical signals. The electrical activity generated by a receptor, called receptor potential, is influenced by its intensity and time course of stimulation. Converting specific stimulus energy into electrical signals is known as stimulus transduction.

The glabrous skin has four types of sensory receptors that detect mechanical

stimuli: Meissner corpuscles, Merkel cells, Pacinian corpuscles, and Ruffini endings (see Figure 2.2). Half of these four receptors are categorized as slowly adapting (SA), as they keep firing when a continuous force is exerted on the skin without any changes in intensity. On the other hand, the remaining two are rapidly adapting (RA) receptors, reacting to movement on the skin but not to stable pressure. Additionally, they vary in size and position on the skin.

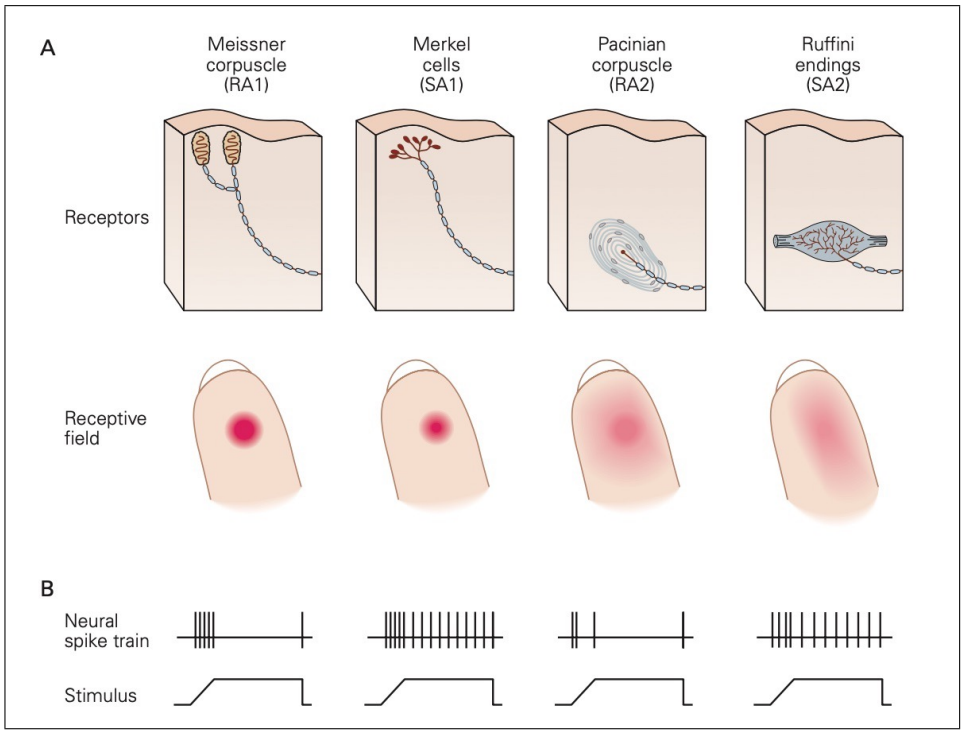

Figure 2.2 Mechanoreceptors are presented in hairless skin. The top row indicates the location of mechanoreceptors within the dermal structure, while the bottom row provides information about the area covered by their receptive fields (spatial scope). The neural firing pattern of these receptors upon receiving a ramp and hold stimulus is also depicted. Reproduced from [1].

Innervation of Merkel cells is carried out by slowly adapting type 1 (SA1) fibers, which convey information about the intensity of pressure applied on the skin. These cells are susceptible to boundary features, angular structures, and points, enabling them to differentiate textures. SAIs are identified by their small receptive fields and irregular, long-lasting firing pattern under continuous stimulus exposure. SAIs respond in a highly localized manner; it is possible to evoke this response only from a small, discrete skin area. The firing rate of SAIs depends on the velocity and amplitude of displacement, and they have low mechanical thresholds. Before a sustained response, there is a period of rapid adaptation. An SAI is exhibiting heightened sensitivity to

stationary indentations and low-frequency vibrations (<8 Hz)[13]. As a result, SAIs contribute to detecting frequencies below 4 Hz[14].

Ruffini endings lead to another type of slowly adapting response, referred to SA type II (SAII). Compared to Merkel cells, Ruffini endings are located deeper in the dermis. Compared to SAI, an SAII has a larger RF, reduced sensitivity to simple skin indentation, a greater sensitivity to skin stretch, and a regular firing pattern under continuous stimulation. The SAII receptors are crucial in perceiving the course of motion or exerted force while the skin is stretched. When an object is moved across the surface of the skin, it results in localized alterations in the shape or configuration of the skin detected by SAII receptors. While SAIs detect localized alterations, SAIIs may convey a neural representation of the stretching stimulus that can be used to determine the movement's direction.

Meissner corpuscles (as shown in Figure 2.2) serve as the terminal structures for rapidly adapting afferent fibers (RA, abbreviated as FAI in humans). They are stimulated when the corpuscle is deformed by pressure. They are positioned within the dermal layer near the epidermis, forming distinctive papillary end organs, and have decreased sizes of the sensory receptive regions.RAs demonstrate a high degree of sensitivity in the vicinity of 40 Hz frequency and are prone to providing temporal information about the stimulus. They produce fewer spikes in the beginning and offset of continuous stimuli, and they can align themselves with a vibratory stimulus and produce one or two spikes during each cycle. Entrainment is characterized by the occurrence of one or more spikes per cycle of stimulation. The rapidly adapting response characteristics of these afferents render them unsuitable for perceiving form and texture; instead, their function may lie in sensing objects sliding across the surface of the hand, thereby transmitting sensory information that enables modulation of grip strength.

The Pacinian corpuscle possesses a distinctive layered structure reminiscent of an onion. The layers that make up the corpuscle are modified types of Schwann cells. It functions as a connective tissue that selectively filters mechanical stimuli at low

frequencies, such as prolonged pressure exerted on the skin. They are found within the deeper layers of the dermal tissue as Ruffini endings and have large RFs. Vibrations between 100 and 300 Hz frequencies are most likely to stimulate the Pacinian corpuscles[15]. Studies have demonstrated that sinusoidal inputs can induce sustained firing in Pacinian corpuscles. Moreover, at the beginning of a stimulus, they exhibit a lower frequency of action potentials compared to rapidly adapting fibers. While Pacinian corpuscles generally respond to higher frequencies, they have the ability to synchronize with vibratory stimuli in the range of 100-150 Hz.

The response characteristics of mechanoreceptor fibers have been extensively investigated in the literature. For example, Güçlü and Bolanowski (2003) studied the ability to detect changes in the stimulus frequency in rapidly adapting fibers of cats by examining the relationship between the mean discharge rate in response to changes in stimulus amplitude and frequency [2]. Figure 2.3 shows the mean firing rate in a cat RA fiber in response to the amplitude of sinusoidal stimulus at 20 Hz and 50 Hz, respectively. The average discharge rate increases in response to the change in the amplitude of stimulus but remains constant in plateau regions. Although the rate-intensity function obtained for each stimulation frequency differs, the general shape is similar, as shown. In addition, the rate-intensity functions at various frequencies of stimulation were utilized to fit using a four-parameter model with different parameters. The analysis revealed that these parameters followed a lognormal distribution.

2.1.2 Rat Primary Somatosensory Cortex

Systems neuroscience strives to comprehend the neural mechanisms that underlie sensory information processing in the brain, specifically how sensory stimuli are encoded as patterns of activity in neurons. In recent years, experimental techniques such as optogenetics and two-photon imaging gained wider accessibility, particularly in rodent studies. As a result, the number of rodent studies increased due to their suitability for these techniques.

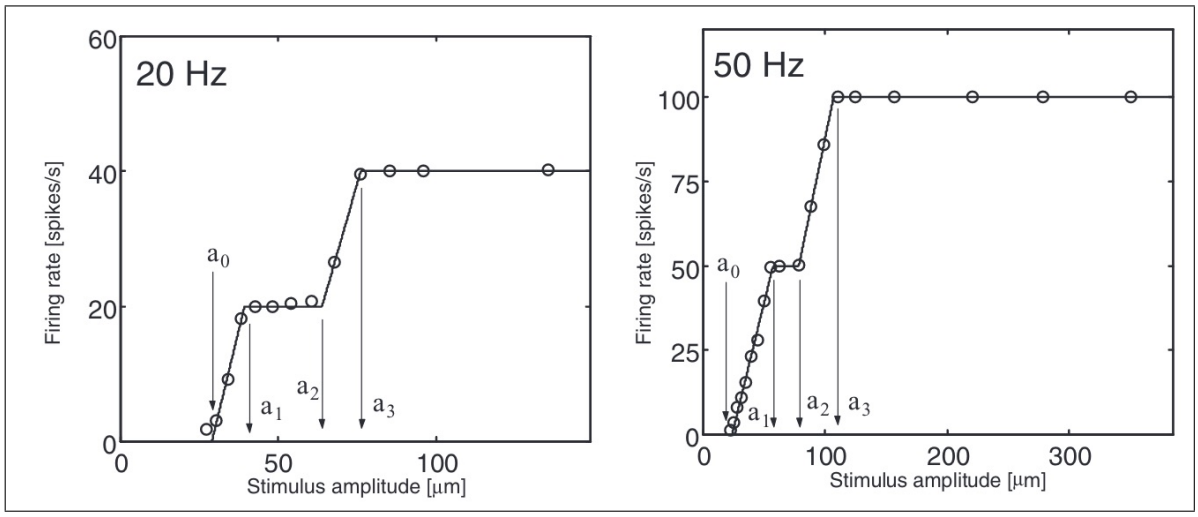

Figure 2.3 The relationship between the mean firing rate and the intensity of stimulation in a cat's rapidly adapting (RA) fiber is depicted. Plots show intensity characteristic parameters (a0-a3) of a cat RA fiber at two different frequencies, at 20 Hz and 50 Hz, respectively.(Adopted from Güçlü and Bolanowski, 2003 [2].

Researchers often turn to the touch system mediated by rodent whiskers as a valuable model for studying key concepts in systems neuroscience. This is due to the system's well-defined neural circuitry and ability to control the stimuli that activate it precisely. Rodents heavily depend on their touch system mediated by whiskers to acquire valuable information about their surroundings. Their whiskers are highly sensitive, allowing them to detect changes in their surroundings and navigate through their environment with great precision, even in complete darkness. This system is crucial for the survival and adaptation of rodents in their natural habitat.

The rat's whiskers, or vibrissae, are organized bilaterally of the rodent's muzzle in a formation resembling a grid. What sets these whiskers apart from regular hairs is the significantly larger follicles they grow from, packed with sensory receptors and nerve terminals. They are arranged within two groups: (i) micro-vibrissae, characterized as shorter and thinner vibrissae located near the apical part of the nose, and (ii) macro-vibrissae, characterized as longer and more rigid mystacial hairs situated behind the micro-vibrissae on the area where whiskers are located [16]. The two types of vibrissae are thought to serve different functions; the macro vibrissae are responsible for transmitting spatial information, as they can move through the surroundings using internal

muscles, while the micro-vibrissae are believed to play a role in collecting fine tactile details to recognize objects and textures[16]. The area around the vibrissa contains mechanoreceptors with varying types, shapes, and distributions, which include Merkel cell-neurite complexes and Ruffini corpuscles [17]. Each of these receptors responds differently to various aspects of tactile stimuli, including amplitude, frequency, time, speed, change in speed, and orientation of whisker movement[18]. Additionally, they have different levels of adaptation. Among these receptors, the dominant ones are the Merkel cells. The vibrissae representation is in the cortex known as the posterior-medial barrel sub-field (PMBSF), which makes up approximately % 20 of the somatosensory cortex [19].

Whisking is a coordinated and cyclical movement of the vibrissae, characterized by repetitive forward and backward motions at approximately 8 Hz [20]. It is associated with the synchronization of different muscle groups, including those involved in respiration and head and nose movements [21]. Berg and Kleinfeld (2003) distinguished two types of whisking: exploratory whisking, which involves sweeping motions that are broad in angle and can last for several seconds, and foveal whisking, which comprises short, high-frequency, small-amplitude sweeps that last for a shorter duration and resemble the organization of photoreceptors in the fovea of the retina [22]. The rhythmic movement of whisking results from the activity of an oscillatory neural network situated within the region of the intermediate reticular formation associated with vibrissa function, the vibrissa-related area in the intermediate reticular formation (vIRt) [23]. This area also receives input from sensory neurons that detect touch and help to regulate the whisking movements.

The rat primary somatosensory (SI) cortex is primarily devoted to processing sensory input from the mystacial vibrissae and is further subdivided into four distinct functional regions, categorized as Par1, also known as the barrel area, along with the areas of forelimb and hindlimb, and dysgranular zone. The presence of barrel structures has been identified in Par1, and in-depth examination using brain slice studies has demonstrated that these barrels are comprised of an aggregation of granule cells, while the peri-granular cortex (septa) acts as the separating entities. The areas encir-

cling the barrel field make up the dysgranular zone, giving rise to functional columns that span multiple layers of the cortex. The cortex is composed of 6 layers, the vibrissae region of S1, specifically Layer IV, is known as the granular zone and contains "barrels" arranged in a somatotopic manner. Each barrel in the vibrissae region contains neurons that respond most strongly and rapidly in response to stimulation of the corresponding whisker, commonly called the "principal" whisker. Studies showed minimal connectivity between neurons of adjacent barrels, resulting in the individual treatment of each barrel as a distinct network [24].

In recent years, significant technological advancements have made functional investigations possible in addition to anatomical studies. By utilizing the power and specificity of genetic studies, it is possible to record and manipulate the electrical activity of the rodent neocortex during trained behaviors. Various recording methods have been modified for conducting awake recordings in rodents, including extracellular unit recordings [25], voltage-sensitive dye imaging [26], and two-photon microscopy [27]. In a study, researchers examined how layer 2-3 of the S1 barrel cortex processes texture coarseness using two-photon calcium imaging [28]. They found that neurons in this area respond to different texture coarseness and are clustered together in the cortex. The study showed that the neural responses of these neurons can be utilized to decipher the roughness of texture, regardless of the specific physical attribute they represent. Comparable results were obtained from different protocols of whisker stimulation, synthetic whisker motions across diverse texture coarseness, and passive presentation of vibrations resembling texture, and both yielded similar results. The study supports that neurons that are responsive to texture are concentrated throughout the barrel field in the S1. The position of an object within the range of a rodent's whiskers can also be roughly identified by the specific whiskers that come into contact with it due to the whiskers being arranged in an array on the animal's face [29]. There are other ways to locate objects using whiskers. As the whiskers move across space, their position can be tracked. When they come into contact with an object, the spikes generated by this contact can be matched with the spatial arrangement of the whisker utilized to deduce the location of the object being touched [30]. Extracting whisker position from afferent responses is another research area actively being pursued [31, 32, 33].

The whisker system of rodents has been the subject of extensive research to unravel the underlying basis of sensorimotor integration and locomotor function[34, 35]. Furthermore, studies of the forelimb and hindlimb areas have also revealed the importance of sensorimotor integration for locomotor control. However, the existing research on limb representations of the rat SI cortex is sparse. In a study examining the organization of excitatory receptive fields in cortical areas related forelimb, findings revealed that even a slight punctuate stimulus can strongly stimulate extensive areas of the somatosensory cortex in the infragranular region, suggesting there is a diverse range of spatiotemporal responses across the somatosensory cortex, which can be used to encode information for tactile discrimination [36]. In a subsequent study, the motor cortex of rats was examined. Researchers aimed to investigate whether the rostral forelimb area of the motor cortex receives somatosensory inputs similarly to the primate premotor or supplementary motor areas. They used voltage-sensitive dye imaging and intracortical microstimulation to map motor representations in the cortex. The results showed that rats' caudal and rostral forelimb areas received excitatory synaptic inputs after forelimb stimulation. This indicates that sensory information processed in the rostral forelimb area may be used to generate coordinated forelimb movements, analogous to the role of the higher-level motor cortex in primates [37].

In another study, researchers investigated the impact of moderate exercise on the somatotopic arrangement of the hindlimb somatosensory cortex (SI) following neonatal thoracic transection. Their findings demonstrate that exercise augmented the proportion of responsive cells in the hindlimb somatosensory cortex (SI) and the strength of their response [38]. Vardar and Güçlü (2017) recorded single-unit spikes to explore the effects of vibrotactile stimulus frequency on AMPA-mediated responses on neurons located in rat S1 cortex [3]. The amplitude of the mechanical stimulus was 100 μ, measured as the peak-to-peak amplitude, on a 0.5 mm static indentation with frequencies of 5 Hz, 40 Hz, and 250 Hz and a duration of 500 ms. Specifically, they examined regular-spiking (RS) and fast-spiking (FS) neurons by calculating the average firing rate (AFR) across two time intervals (100ms from the onset and late 400ms of stimulus duration). As depicted in Figure 2.4, it is evident that within the initial 100 ms, a higher number of spikes are observed across all neurons. Additionally, a clear pattern

of entrainment, characterized by a 1:1 firing ratio, is observed specifically during the 5 Hz frequency stimulation. In contrast, no such entrainment pattern is discernible during the 40 Hz and 250 Hz stimulations.

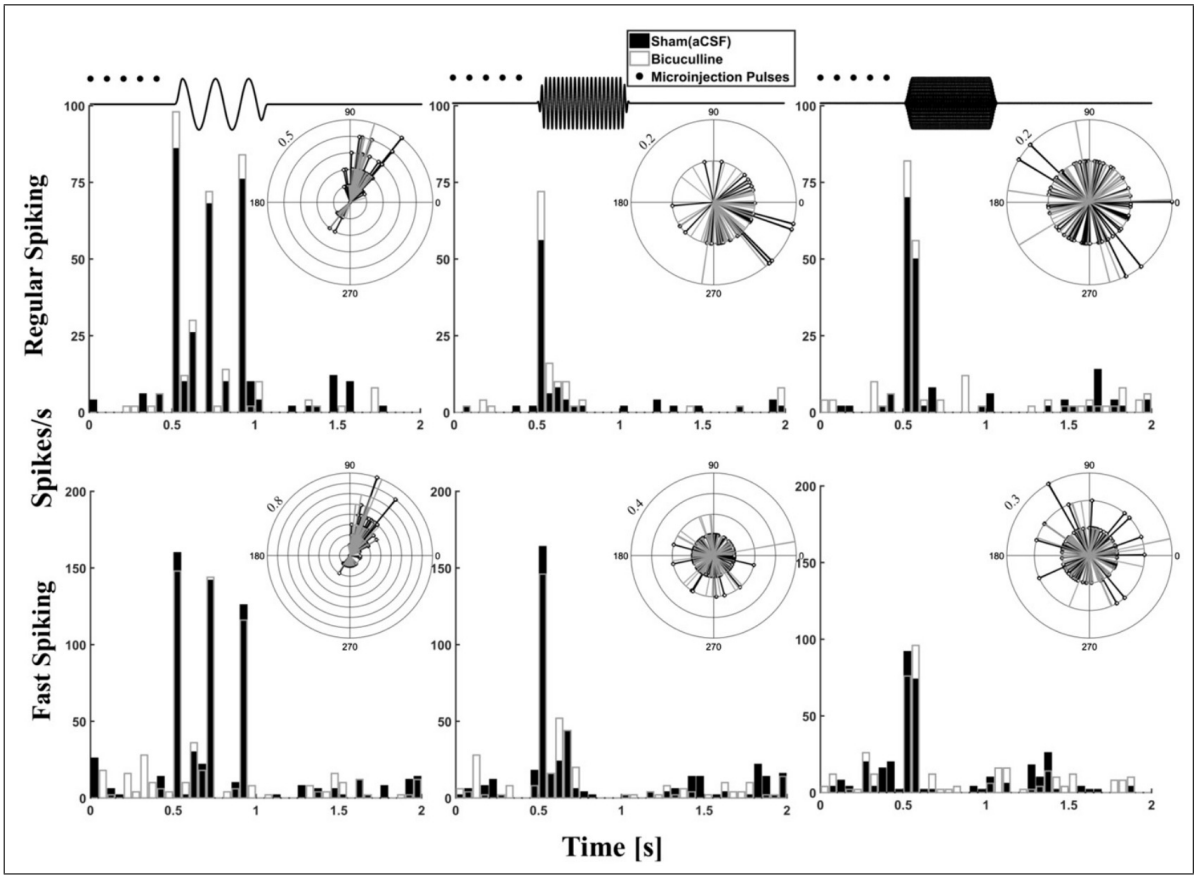

Figure 2.4 Spike histograms are depicted. The stimulus waveform is shown above the PSTHs; black bars correspond to the condition of the sham, while white bars represent the bicuculline application.(Reproduced from Vardar and Güçlü, 2017 [3].

Further research is needed to improve our understanding of sensory and motor functions within the sensorimotor cortex. The trunk motor cortex must also be understood in relation to other sensory cortices. This knowledge gap is crucial, especially in the context of recovery and learning following neurological injury or disease. For instance, the recent study aimed to comprehend the somatotopic organization of the trunk motor and sensory cortices and the synthesis of sensory and motor functions in the trunk cortex [39]. To accomplish this, the researchers used electrophysiological mapping to identify the location of thoracic dermatomes and their corresponding representation in trunk S1. In addition, they used intracortical microstimulation to

examine trunk M1 function and organization. Then, they assessed sensorimotor integration by analyzing somatosensory evoked potentials across a wide area of the sensorimotor cortex. They also performed retrograde tracing to determine the pathway of somatosensory input. Lastly, to comprehend the functional importance, they recorded single units in trunks S1 and M1 upon encountering unexpected postural disturbances. Mapping studies have demonstrated significant topographical arrangement of the trunk primary somatosensory (S1) and primary motor (M1) cortices. The integration of sensory and motor functions between the trunk and hindlimb systems was extensive. These studies suggest that thalamocortical projections are central in integrating hindlimb somatosensory information with trunk M1. These findings shed light on the integration and processing of sensory information during posture control. These findings can contribute to the advancement of efficient rehabilitation strategies for patients with spinal cord injuries. As a result, the study provided a comprehensive understanding of the cortical organization and its functional relevance while demonstrating how the trunk and hindlimb interact preferentially.

2.2 Recording Electrical Activity of the Brain

Hans Berger, a renowned German psychiatrist, is credited with the discovery of the electrical activity of the brain through electroencephalography (EEG) recordings in the late 1920s [40]. He observed that when subjects opened their eyes, the neural oscillations within the alpha frequency range (8-13 Hz) in EEG recordings decreased in amplitude or disappeared entirely. The observation made by Hans Berger was vital because it demonstrated a connection between the alpha rhythm and the state of the observer. Many scientists and physicians have observed this phenomenon, recognized as the "Berger effect" or "alpha blocking," since Berger's initial discovery [41].

When the multiple cellular processes produce an electric current in a specific brain area, they superimpose and produce an electric potential termed V_e (a scalar measurement in Volts) in the surrounding extracellular medium at that location [6]. By placing electrodes outside of the brain, it is possible to monitor electric fields with

high time resolution (less than a millisecond), which can provide valuable information about various aspects of how neurons communicate with each other. The electrical activity of neurons can be measured at different scales. Conventionally, the electrical signal, V_e, obtained from scalp recordings has been known as the electroencephalogram (EEG). For example, the recorded electrical activity is called the electrocorticogram (ECoG) when electrodes are positioned on the cortical surface. On the other hand, when small electrodes are inserted within the brain, it is known as the local field potential (LFP), also referred to as intracranial EEG. Additionally, both single-unit and multi-unit spikes can be measured by using even smaller intracranial microelectrodes. Figure 2.5 shows how the EEG, ECoG, LFP, single-unit, and multi-unit activity techniques differ from each other based on where they are recorded from. Any excitable membrane, such as dendrites, axons, or axon terminals, and transmembrane currents contribute to generating the extracellular field. It is created by combining all ion-mediated mechanisms, including fast action potentials and slow fluctuations in glia [6].

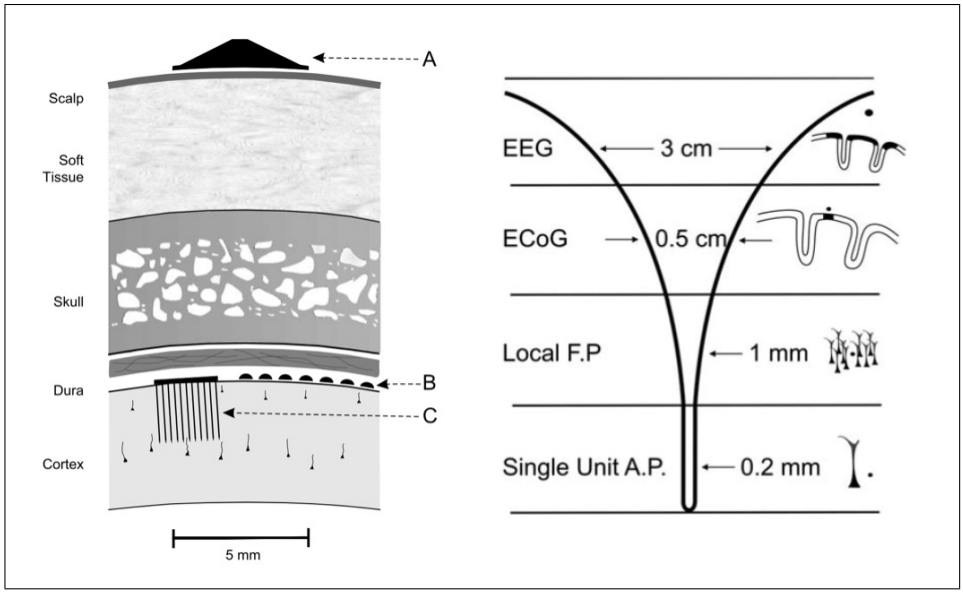

Figure 2.5 Various methods are used to quantify the brain's electrical activity are shown. (a) Depicts different scales such as EEG (A), ECoG (B), and single/multi-unit recordings (C) Reproduced from [4]. (b) Shows the part of recorded electrical signals. Modified from [5].

Typically, broadband recordings, such as EEG and ECoG, are generally categorized into spectral bands, including delta (<4 Hz), theta (4 to 8 Hz), alpha (8 to 12 Hz), beta (12 to 30 Hz), gamma (30 to 80 Hz) and high gamma (80 to 150 Hz).

However, the nomenclature of these bands may not be consistent across studies, as the boundaries defining each band can vary slightly between them.

2.2.1 EEG

Electroencephalography (EEG) is the widely practiced and oldest method for monitoring brain activity in clinical and research settings. One of the main advantages of EEG is its non-invasive recording procedure. Placing electrodes directly on the scalp makes the application of EEG easier than other invasive methods. In general, the electrical activity recorded using EEG is not closely related to the spiking activity of single neurons. This is mainly due to the physical barriers posed by the soft and hard tissues between the current source and the recording electrode.

EEG measures the electrical activity arising from the concurrent activity of numerous neurons in the brain. The most frequent types of neurons in the cortex are the pyramidal neurons, about %80 of all neurons in the cortex have a characteristic orientation that generates perpendicular electrical dipole configurations with respect to the cortical surface. This means that the electrical potentials generated by these neurons are more easily detected by the EEG when located in the gyral tissue (the raised, folded areas of the brain's surface) compared to the sulcal tissue (the grooves between the gyri). As a result, EEG recordings tend to be more sensitive to the activity of neurons in the gyri than those in the sulci.

Historically, initial studies of EEG focused on epileptic manifestations and the demonstration of epileptic spikes. Grey Walter's identification of the delta focus, which appears over brain tumors, led to exploring additional connections between focal EEG patterns and brain lesions [42]. During the late 1930s, investigations of EEG patterns in patients with metabolic disorders, particularly hypoglycemia, were carried out concurrently with this research [43]. Meyers et al. [44] conducted the initial use of implanted intracerebral electrodes for depth EEG in humans in the late 1950s at the University of Iowa. These recordings were utilized to examine the EEG activity of the basal ganglia

and thalamus in patients with basal ganglia dyskinesias and epilepsy. Kleitman and his collaborators discovered rapid eye movement sleep in 1953 [45]. This has been made possible by advancements in intracerebral EEG recordings, computational techniques, and microelectrode recording methods.

EEG provides valuable insights into numerous neurological disorders. Over the past 30 years, the significance of EEG has increased in intensive care settings. Identifying and revealing nonconvulsive seizures or nonconvulsive status epilepticus, detecting alterations in focal EEG background activity associated with acute brain lesions, and nonepileptic encephalopathies require using EEG. As a result, continuous EEG monitoring (cEEG) has become increasingly common in intensive care units in recent years. In addition to identifying seizures, certain EEG features, including slowed brain activity and nonepileptic episodic transients, indicate particular underlying causes and offer critical prognostic information for patients with acute nonepileptic encephalopathy. Recent research has demonstrated that combining clinical assessment with EEG background reactivity provides the most reliable prognosis for postanoxic coma [46].

In addition to its clinical applications as a diagnostic tool, various aspects of EEG, including signal magnitude, power spectral densities, temporal and frequency characteristics, and autoregressive parameters, have been utilized for feature extraction. The P300 wave has been used in a number of studies to examine the mental processes associated with gamma responses. This peak usually appears in the event-related potentials (ERPs) when subjects encounter unexpected or rare "oddball" stimuli or when a "target" stimulus is missing from a sequence of standard stimuli. By using missing auditory stimuli as a target, scientists have detected a P300 component with a frequency of 40 Hz in the cat's hippocampus, reticular formation, and certain cortical areas. This response is observed around 300 milliseconds after the stimulus and is accompanied by a slow wave at 4 Hz [47]. Different types of stimulation, including auditory and visual cues, are used to control brain-machine interfaces (BMIs) via P300. The P300 speller is a well-established tool that enables individuals experiencing locked-in syndrome to communicate with the world beyond their physical limitations [48, 49].

Using the frequency properties of the recorded signal is another approach for controlling BMI with EEG. For BMIs, motor imagery (MI) is a popular tool to decipher brain signals. The frequency components of electroencephalographic signals (EEG) in alpha (8-12 Hz) and beta band ranges (12-32 Hz) [50], or delta band ranges (0.1-4 Hz) [51] are often used to extract features from motor imagery. Nevertheless, a limited number of studies specifically investigate the gamma frequency bands(32-100 Hz). A recent finding suggests that the gamma band may be associated with gait attention [52]. Ortiz et al. have offered an innovative brain-machine interface paradigm that has been established, focusing on the activity during mental tasks involving MI. Furthermore, they demonstrated the feasibility of a gamma band-based approach to control the exoskeleton.

2.2.2 ECoG

In 1950, neurosurgeons W. Penfield and H. Jasper pioneered ECoG as a crucial component of their revolutionary Montreal procedure, aimed at identifying epileptogenic zones and treating severe epilepsy[53]. It involves placing electrodes made of platinum-iridium or stainless steel material directly on the cerebral cortex surface. To record ECoG signals, part of the skull must be removed to reach the cortex. This way, the electrodes can directly record the brain's electrical activity without interfering with the skull or other tissues. The ECoG is less invasive than intracortical recording because it does not harm the parenchyma of the brain. Additionally, ECoG provides a higher spatial resolution, and usually, filtering effects are rare compared with EEG, which allows it to preserve more of the frequency content of the electrical signal, as shown in Figure 2.6.

The electrocorticography (ECoG) technique is gaining popularity for studying multiple cortical phenomena in clinical settings. These electrodes are primarily utilized in epilepsy surgeries to identify the areas of the brain responsible for epileptic activity before surgery and to confirm the operation's success by checking whether any remaining epileptiform activity is left during the surgery.

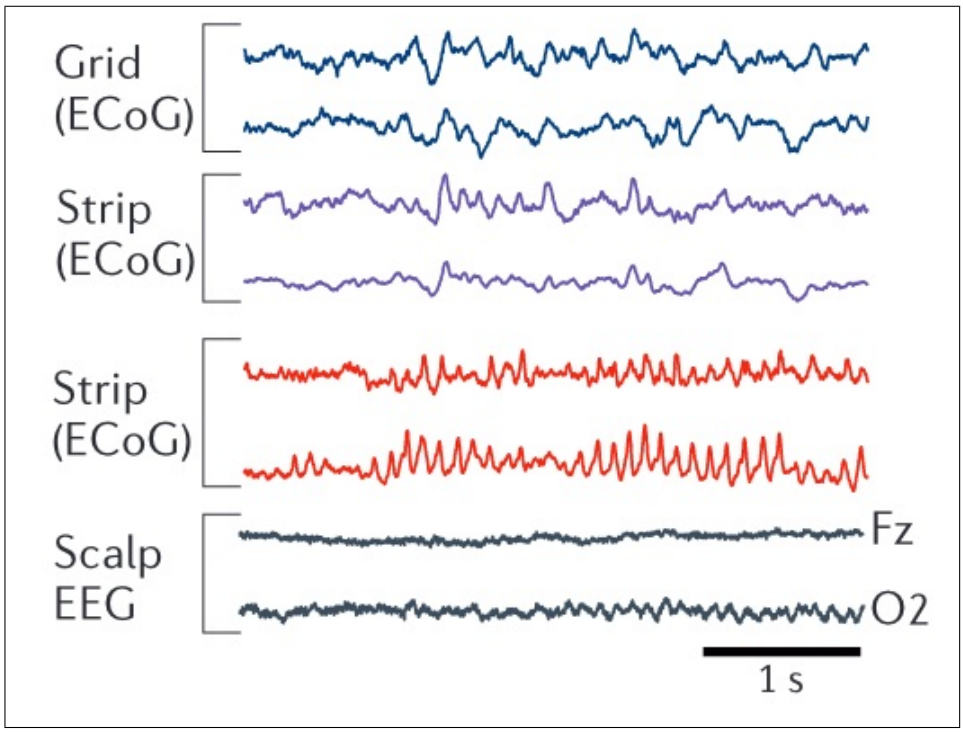

Figure 2.6 Simultaneous recording was conducted using a subdural grid array consisting of three electrodes positioned over the left temporal cortex and using a strip that has 8 contacts placed on the surface of the left hemisphere (recording ECoG signals), and in a patient with epilepsy, scalp electroencephalography (EEG) was performed over both hemispheres (fz and O2). Compared to scalp EEG, ECoG signals are larger in amplitude and have a greater resolution at higher frequencies. Modified from [6].

The potential utilization of ECoGs in BMI applications was investigated by gathering information from patients implanted with ECoG electrodes to identify epileptic activity zones. BMI technologies can recover motor functions of people with motor disabilities. Consequently, BMIs designed for movement restoration typically interpret neural signals from motor-related brain areas. However, in a recent study, Cho et al. developed a brain-machine interface (BMI) system that integrates gamma band ECoG signals recorded from the S1BF cortex using a four- channel electrode with electrical stimulation to provide reward-based feedback [54]. These signals were processed to extract BMI signals. Then they used these signals to control the movement of a dot on the screen. A power spectrum in the gamma band of 40-70 Hz was determined according to previous literature. Neural activity was recorded from the S1BF cortex of rats using four-channel ECoG electrodes. Researchers demonstrated successful learning of one-dimensional dot movement on a screen through neural control, with medial forebrain bundle (MFB)stimulation provided as a virtual reward for task completion. This

means that somatosensory cortex activity is modulated by higher cognitive functions. The results of their study indicate BMI technology that utilizes electrocorticographic signals holds significant potential for a wide range of applications.

2.2.3 Local Field Potentials

Local field potentials (LFPs) are the coherent electrical activity that emerges from neurons located in close proximity to each other. There are varying explanations about the frequency spectrum of the LPFs in the literature; however, it can be broadly described as the low-frequency activity of the neurons (< 500 Hz).

LFPs reflect the gradual neural activity arising based on the dynamics of the interplay between current sources and sink within the brain's neural network. To investigate electrical activity originating from deeper regions, various tools such as metal or glass electrodes and silicon probes can be employed to measure LFP. Capturing a signal with a broad frequency range (DC to 40 kHz) using a microelectrode provides valuable information for examining cortical electrogenesis. It includes variations created by APs and fluctuations in membrane potential within a confined neuronal space [6]. Numerous observation points, closely spaced recording locations, and minimal disruption to brain tissue are required to attain high spatial resolution. With an adequate density of recording sites, monitoring the spiking activity of most or a significant portion of neurons within a limited volume is possible. The field has advanced rapidly due to the development of silicon-based micromachined probes with an increasing number of recording sites [55].

Pyramidal cells, a class of excitatory neurons in many brain regions, have parallel dendrites, creating an ideal geometry for forming strong dipoles. Consequently, the electrical activity of these cells can generate a strong LFP signal. In contrast, other types of neurons, such as those with a closed field arrangement, have more radially distributed dendrites, leading to cancellation effects that reduce the strength of the LFP signal. Overall, the geometry of dendritic arborization is an important factor

that can influence the strength and spatial distribution of the LFPs in a designated area of the brain. The generation of current dipoles and the resulting LFP signals is a complex process involving the interplay of many different factors, including excitatory and inhibitory synaptic inputs, subthreshold membrane oscillations, and post-spike afterpotentials [56].

Numerous studies have investigated the frequency-dependent characteristics of LFPs in different areas of the brain and under different experimental conditions. Ray et al. investigated the different origins and functional roles of gamma and high-gamma activity in macaques using local field potential (LFP) recordings. They examined the spectral characteristics of visual evoked potentials. They found that gamma activity was modulated by feedforward inputs and originated primarily from layer 4 of the visual cortex, where it was strongly correlated with spiking activity. In contrast, high-gamma activity was modulated by feedback inputs and originated from layers 1-2 of the visual cortex. The correlation between gamma activity and spiking activity in layer 4 supports the idea that gamma oscillations are produced by the interaction of excitatory and inhibitory input signals that drive synchronized firing of local neuronal populations [57].

LFPs were also utilized to decode motor activity. Mehring et al. investigated the characterization of the direction of movement in diverse frequency bands of LFPs recorded from monkeys' motor cortices. They found that LFPs in the beta (15-30 Hz) and gamma (30-90 Hz) frequency ranges were most strongly modulated by movement direction. In contrast, theta (4-8 Hz) and alpha (8-15 Hz) frequency ranges were weakly modulated by movement direction. The study provided insights into the frequency-specific neural coding of movement direction in the motor cortex and highlights the potential utility of beta and gamma activity in LFPs for decoding movement direction in brain-computer interfaces [58].

2.2.4 Action Potentials

The action potential is a transient depolarization and repolarization of the membrane potential at a specific site in an excitable cell, such as neurons, muscle cells, and some plant cells. In the 1920s and early 1930s, Edgar Douglas Adrian and Yngve Zotterman made one of the earliest documented recordings of action potentials [59]. Utilizing a capillary electrometer and a 3-stage amplifier, they conducted measurements and analyses of action potentials originating from sensory nerve endings and peripheral nerve fibers. In the early 1950s, Alan Hodgkin and his colleagues demonstrated that the activation and inactivation of ion channels in the neuronal membrane causes the action potential [60]. They proposed a model, a breakthrough in neuroscience, that provided a quantitative framework for understanding the electrical properties of neurons. The Hodgkin-Huxley model, is a mathematical framework that explains the initiation and transmission of neural impulses in neurons. It is comprised of a system of nonlinear differential equations that approximates the electrical properties of excitable cells. Hodgkin and his colleagues developed a voltage clamp technique that was critical in investigating the ionic basis of nerve conduction. Using the voltage-clamp technique, they precisely controlled the voltage across the neuronal membrane and measured the ionic currents that flow across the membrane during an action potential.

Recent advancements in neuroscience techniques, such as single-unit recordings using microelectrode systems, have enabled the examination of single-unit activity in the brain. A microelectrode is surgically implanted in the brain and can record alterations in voltage over time. Glass micropipettes and metal electrodes are frequently employed for single-unit recordings.; glass micropipettes and metal electrodes. Glass micropipettes are highly resistive and have low capacitive properties, making them well-suited for measuring resting membrane potentials and action potentials. However, they are not suitable for measuring extracellular signals. On the other hand, metal electrodes are usually made from tungsten or stainless steel wires and have a thin, insulated shaft. Their lower impedance at the spectral band of spike signals results in a higher signal-to-noise ratio than glass micropipettes. This makes them ideal for measuring extracellular spikes and allows for more precise and reliable measurements

of neural activity [61]. Although stainless steel and tungsten microwires continue to be utilized in current research, they have some disadvantages. As they are penetrating electrodes, due to their potential to induce bending and elicit foreign body reactions at the site of implantation, they can cause a gradual degradation of the signal-to-noise ratios (SNRs). Unlike microwires, thin-film arrays offer the advantage of having multiple active sites, allowing for precise and maintained distances between each site during implantation. In the literature, researchers have studied a range of materials for electrode construction, including silicon, metal, ceramic, and polymer-based materials.

It has been shown that BMIs can restore function to patients who have been paralyzed or suffer from neurological diseases. However, the technology is not yet clinically available due to the issue of signal reliability and consistency, as recording signals over an extended period of time poses challenges. This failure is commonly attributed to chronic inflammatory responses in the vicinity of the electrode that cause neurodegeneration, which damages neurons that can be recorded [62]. To assess the feasibility of neural prosthesis systems using neural activity from chronically implanted intracortical microelectrode arrays, Simeral et al. designed a pilot clinical trial to test the BrainGate BMI system [7]. The trial raised questions about implanted electrodes' longevity and reliability in recording neural signals and their effectiveness in controlling assistive technologies and enabling functional electrical stimulation. A study was conducted to assess the control capability of the neural cursor and system characteristics of BrainGate over the course of five consecutive days using a set of 100 microelectrodes placed on a 4x4mm array implanted in a patient's motor cortex. A closed-loop point-and-click cursor control system was developed using a Kalman velocity decoding filter and a linear discriminant click state classifier, both based on population-level neural activity. This enabled time-amplitude sorting of neuronal spiking activity. They determined the spiking activity of the neuronal population involved in cursor control to investigate if the defining properties of motor cortex (MI) neurons persisted after a long time interval following implantation, as shown in Figure 2.7.

As a part of the Radial-8 evaluation task, the firing rates of numerous units were found to be significantly modulated in response to the intended direction of cur-

sor movement. The population of tuned units exhibited preferred directions, as shown in Figure 2.7 (c), even though the distribution was not uniform on any of the assessment days ($P > 0.05$). The non-uniformity of the distribution of tuned units was emphasized by quantifying the count of preferred direction falling within each of the eight 45-degree bins, as shown in Figure 2.7 (c). Participants achieved an average task performance of $91.3\% \pm 0.1\%$ correct target gain for both tasks. Moreover, local field potentials, electrode impedances, and unit waveforms were monitored on a daily basis to characterize the neural interface system. The results of the study showed that spiking signals were successfully decoded from 41 out of 96 electrodes over a span of five days, indicating that the BMI system can offer reliability for patients with tetraplegia, even after 1000 days since implantation.

2.3 Psychophysical Methods for Measurement of Sensation

Gustav Fechner was a German philosopher, physicist, and experimental psychologist considered the founder of psychophysics. In 1860, he published his seminal work in Leipzig, "Elemente der Psychophysik," which introduced the fundamental concepts and methods of psychophysics [63]. The term "psychophysics," coined by Fechner, describes the scientific study that focuses on the relationship between physical stimuli and subjective conscious experiences, including sensations and perceptions. Fechner believed measuring subjective experience using objective, quantitative methods was possible and developed several experimental techniques.

Psychophysicists typically use stimuli like pure tones, lights, or mechanical pressure as they can be objectively measured. It has been applied to all sensory domains, including visual, auditory, and tactile perception. The research typically focuses on three main areas of investigation: absolute thresholds [64, 65], discrimination thresholds [66, 67, 68], and scaling [69, 70]. The absolute detection threshold can be defined as the lowest amplitude level at which a stimulus elicits a response. The discrimination threshold refers to the minimum difference between two stimuli in a particular dimension, such as amplitude, frequency, and duration, that an observer can perceive as

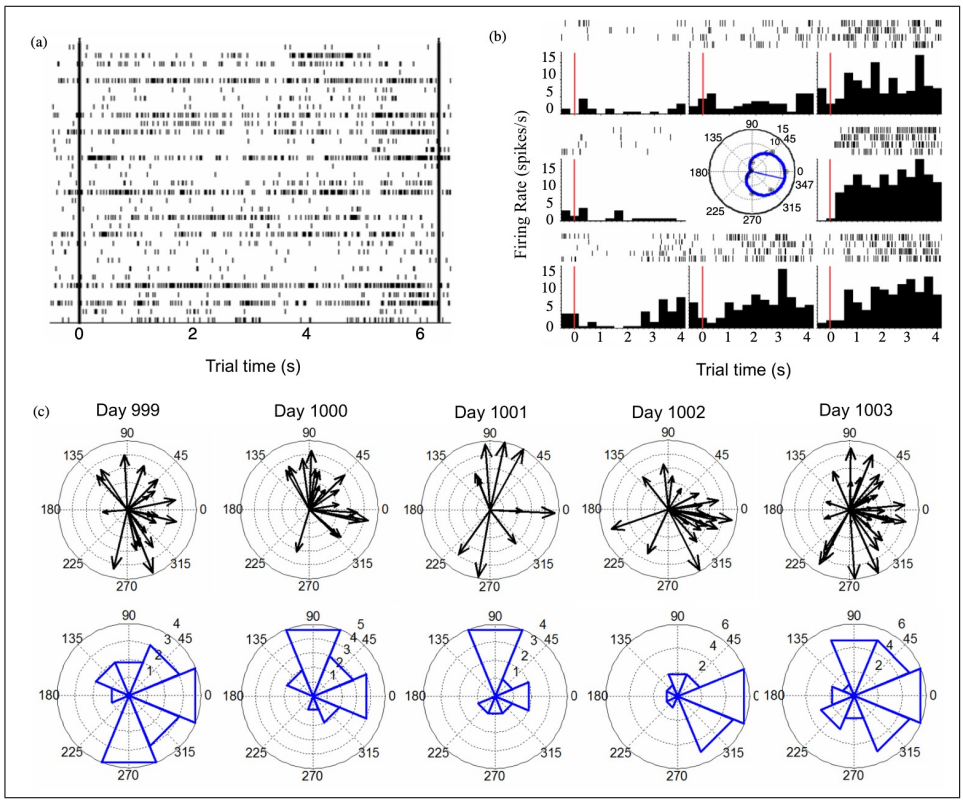

Figure 2.7 Tuning characteristics of spikes while subjects control the neural cursor. (a) A raster plot showing spiking patterns of 33 units recorded simultaneously while performing neural cursor point-and-click and the Radial-8 tasks on Day 1000. The trial began at time 0 (indicated by the left perpendicular line) and ended at 6.18 s (indicated by the right perpendicular line). (b) Spike activity of a neuron while the subject does the Radial-8 task. For each of the eight directions of movement, a tick represents the spike activity, and a movement is depicted by each row of ticks. Histograms show spiking activity across trials. c) The top row displays the tuning of all the neurons in relation to the direction of the movement; the radius of the circle corresponds to a modulation depth of 1. The bottom row depicts the unit counts tuned significantly in eight different cardinal task directions, presented within 45-degree bins. Reproduced from [7].

distinguishable. In scaling experiments, subjects are asked to assign numerical values to their experiences, such as the degree of intensity perceived for a particular stimulus.

Psychophysical studies focusing on touch have been conducted to explore how the central nervous system processes tactile information and how we perceive such information. Different tactile stimuli (e.g., ramp-and-hold, gratings) have been employed in the literature; however, the vibratory stimuli have been the most popular ones. The ease of controlling stimulation parameters such as amplitude and frequency and the frequency-specific sensitivity of peripheral mechanoreceptive afferents (such as the greater sensitivity of PCs to high frequencies and the sensitivity of RAs to flut-

ter stimuli) makes them useful in experimentation. Building upon this physiological framework, researchers have established psychophysical channels for glabrous touch to gain deeper insights into how various mechanoreceptive afferents transmit information [71].

2.3.1 Four-Channel Model in Tactile Psychophysics

Bolanowski et al. (1988) hypothesized that four psychophysical channels are dedicated to the sense of touch. These are, respectively; Non-Pacinian I (NPI) channel is mediated by RA (FAI) fibers innervated by Meissner corpuscles; the NPII channel is governed by SAII fibers innervated by Ruffini endings; the NPIII channel is controlled by fibers called SAI innervated by Merkel's discs. Finally, the Pacinian (P) channel is mediated by PC (FAII) afferents innervated by the Pacinian Corpuscles. These channels were defined based on studies in the literature about response properties of mechanoreceptive afferents and tactile psychophysics [72]. According to the proposed framework, each tactile psychophysical channel is responsible for conveying information within a specific range of frequencies [71]; the NPI channel is responsible for transmitting flutter sensation within the spectral range spans from 2 to 40 Hz, whereas the P channel transmits the sensation of vibration within the range of 40-500 Hz. Similarly, the NPII channel is believed to mediate a "buzz-like sensation" in the 100-500 Hz range, while the NPIII channel is responsible for transmitting the sensation of pressure within the 0.4-2 Hz range [71]. While the most sensitive channel at a particular frequency may be responsible for transmitting sensations around the threshold levels, higher amplitudes of stimulation can activate other channels, leading to the perception of sensations that are influenced by the combined contributions of multiple channels. Sensory channels are characterized by their unique frequency ranges, the specific sensations they elicit, and their diverse response properties that can vary depending on the nature of the stimulation. For instance, temporal and spatial summation properties are only present in the P channel among all channels. As the duration of the stimulus increases, there is a decrease in the detection threshold; this is called temporal summation. In contrast, the spatial summation indicates a negative correlation between the

detection threshold and the stimulated area. It is important to note this four-channel model mostly explains psychophysical responses to threshold-level stimuli.

2.3.2 Masking

Masking is a term used to describe various phenomena in which the presentation of a mask stimulus can hinder the performance of a task that involves making a judgment or evaluation about another stimulus, known as the target [73]. The masking paradigm is a widely-used technique in cognitive neuroscience and experimental psychology to study cognitive processes such as attention, perception, memory, and consciousness [74].

As shown in Figure 2.8, the most frequently employed masking paradigms are the forward masking technique, where the masking stimulus is presented before the test stimulus; the backward masking technique, where the masking stimulus is presented after the test stimulus; and the simultaneous masking technique, where the masking and test stimuli are presented simultaneously.

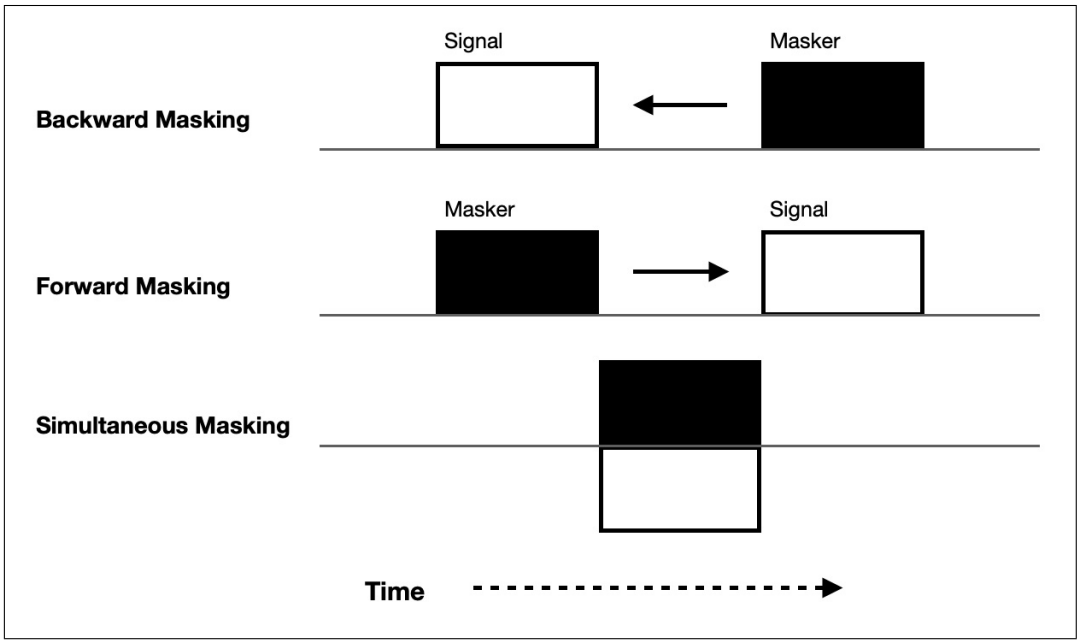

Figure 2.8 Illustration of backward, forward, and simultaneous masking. Reproduced from [8].

As mentioned before, masking paradigms have been frequently used in different domains in the literature. In the realm of visual masking, the phenomenon is often categorized into two types, distinguished by the spatial relationships between the target contours and patterns of masks. When masking occurs through the spatial overlapping of contours, it is commonly called "pattern masking." On the other hand, when masking stimuli include consecutive but non-overlapping contours, it is termed "metacontrast"[75]. In metacontrast masking, the temporal gap (the time period without stimulus) between the presentation of both stimuli can vary significantly, being either very brief or prolonged. However, at intermediate temporal gaps, the perception of the target is hindered, resulting in a target visibility-versus-temporal gap relationship that follows a U-shaped pattern. One proposed mechanism is that the neurons responsible for representing the contours of the target and mask have inhibitory interactions with each other [76]. According to this theory, the presentation of shapes triggers two different neural responses in two different channels; they are respectively characterized by a fast response and short duration and a slower response but longer persistence. The fast-acting channel is tasked with conveying transient events associated with the stimulus, specifically referring to its onset and offset. In contrast, the slower channel carries persistent signals about the shape and color of the stimulus. Few studies investigated the electrophysiological relevance of metacontrast masking, and they reported a modulation in ERPs following the onset of the target about 200 milliseconds after metacontrast suppression [77].

In the tactile domain, the presentation of a vibrotactile stimulus may potentially disrupt the perception of another stimulus. This disruption, referred to as masking in the tactile domain, results in the suppression of perception. The quantitative equivalent of this scenario is the elevated detection thresholds and impeded localization or identification of the affected stimuli as observed in psychophysics studies [66]. Although the underlying neural mechanism is not fully known, masking stimulation is thought to be effective by altering the SNR in the cortex [78]. Several factors influencing the degree of masking have been documented, including the amplitude, frequency, and duration of both the test stimulus and the masking stimulus and the temporal gap between the two stimuli [9, 79].

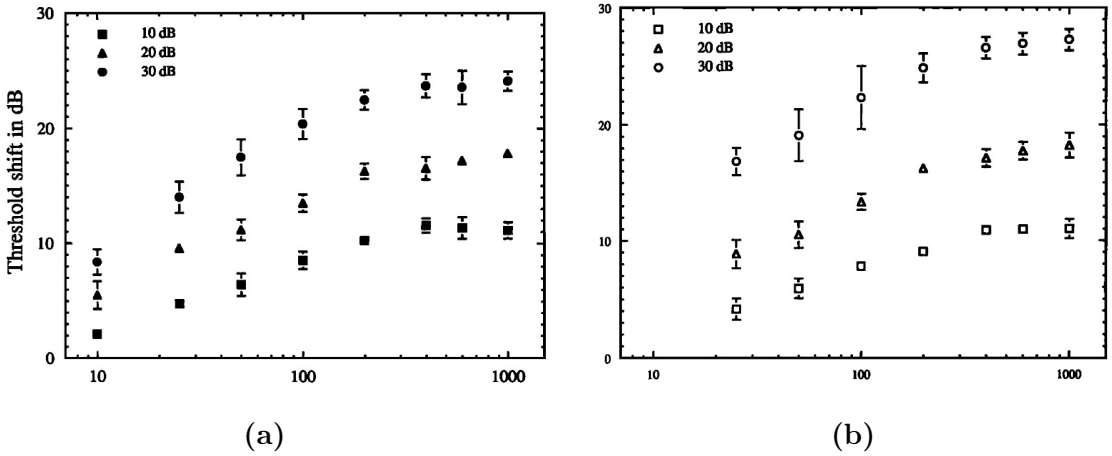

Figure 2.9 Mean threshold shifts are depicted as a function of masking stimulus duration; the x-axis represents the duration of the masking stimulus in ms. (a) illustrates the shifts in thresholds obtained with 250 Hz stimulation, where the amount of masking significantly increased with increasing duration and amplitude of the masking stimulus ($p < 0.001$, $p < 0.01$), respectively. (b) Similar functions were obtained for the 20 Hz stimulation, where the amount of masking increased with both the duration and the level of the masking stimulus ($p < 0.0001$). Reproduced from Gescheider et al., 1995 [9].

Gescheider et al. (1995) conducted two experiments to examine the effects of the duration of masking stimulus and amplitude in the forward masking paradigm, specifically by focusing on P and NP1 channels [9]. The temporal gap between the masking and test stimulus and their frequencies was constant. The duration and amplitude of the masking stimulus were systematically changed in different experiments to investigate their effects, as seen in Figure 2.9. The masking and test stimuli were at the same frequency, specifically 20 Hz and 250 Hz. It was observed that the threshold shift, indicating the amount of masking, increased with both the duration and level of the masking stimulus for the respective tested frequencies. Notably, the study demonstrated that while the NP I and P channels exhibited comparable responses to variations in masking duration and amplitude, the NP I channel displayed greater sensitivity to amplitude alterations in masking stimulus and exhibited higher susceptibility to masking compared to the P channel.

Gescheider et al. (1995) also conducted a study examining temporal parameters. Absolute thresholds were measured to detect a 250 Hz test stimulus at different temporal gaps and durations following the offset of a 250 Hz masking stimulus. The findings revealed that the masking effect decreased proportionally to the test stimulus

duration and the temporal gap between masking and the test stimulus [79].

3. METHODOLOGY

3.1 Subjects

We used seventeen healthy Wistar Albino rats (10 females and 7 males) in experiments. The distribution of age and weight of the subjects by sex can be seen in Figure 3.1. The mean age was 6.37±1.08 months, and the mean weight was 310.11±91.8 gram. The experimental protocols were granted ethical approval by the Institutional Ethics Committee for the Local Use of Animals in Experiments at Boğaziçi University.

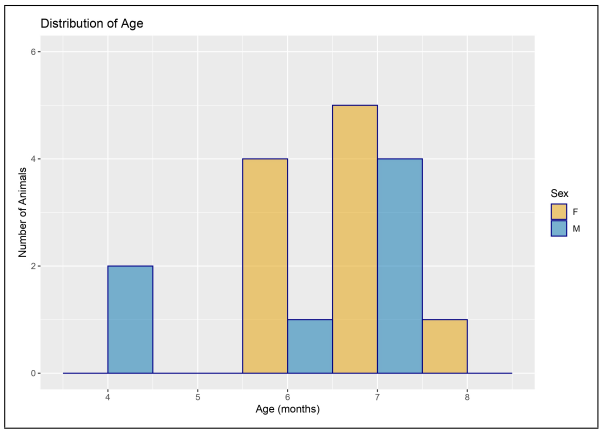

(a)

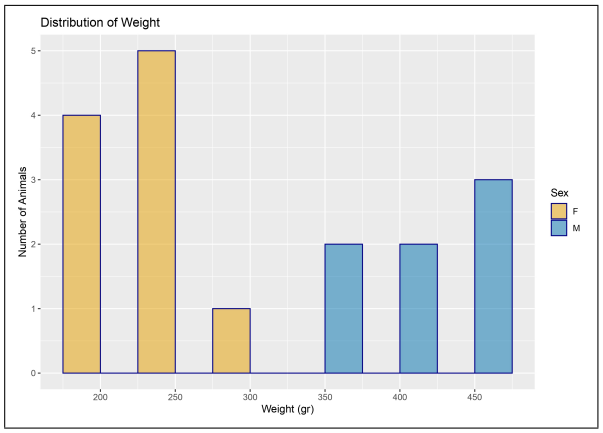

(b)

Figure 3.1 Distributions of subjects are shown. (a) represents the age distribution, and (b)represents the weight distribution.

3.2 Apparatus

Figure 3.2 outlines the experimental setup. MATLAB, R2008a (Math Works) software was utilized to gather and analyze data. Custom MATLAB scripts were used to produce stimulus waveforms and to record electrode voltage readings in time-series format. The MATLAB code controlled experiment parameters, including frequencies of stimuli, level of attenuation, number of trials per attenuation level, the timing of delivery, and length of trials. USB-6251 DAQ card (National Instruments) was used to convert the MATLAB-generated stimulus waveforms into analog signals.

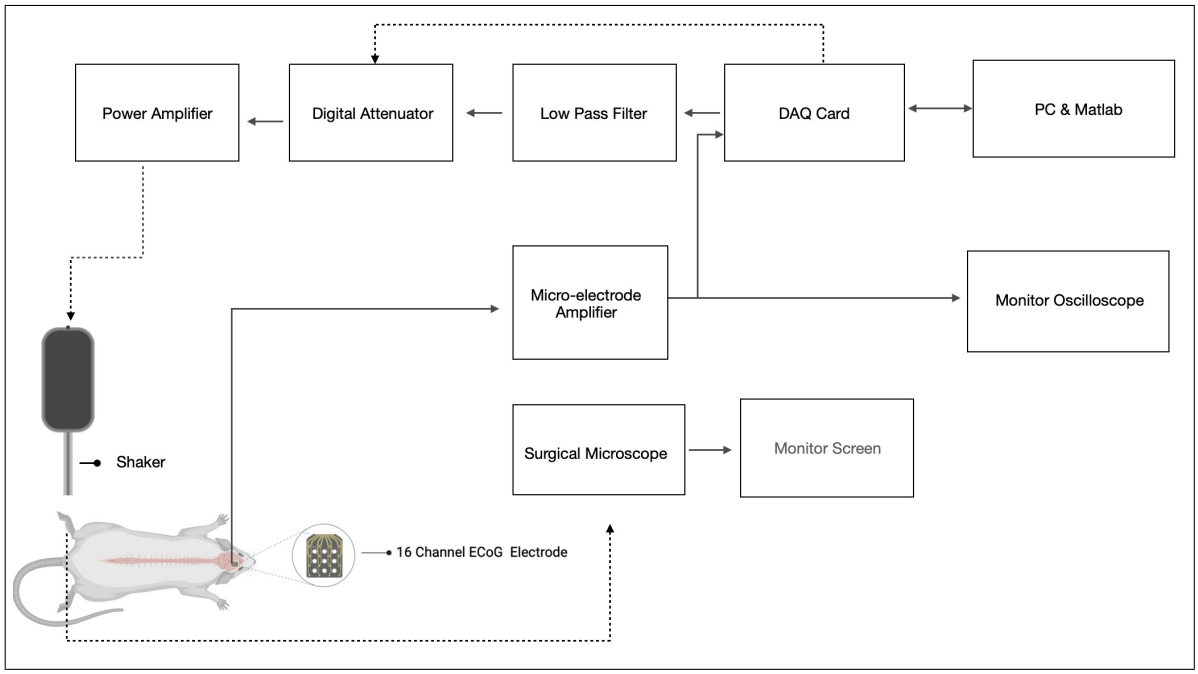

Figure 3.2 The diagram of the experimental setup is depicted. Modified from [10].

To reduce noise, the custom-made 1-kHz low-pass filter was utilized to filter the analog signal for stimulus waveform. The signal was then attenuated using a MATLAB-controlled digital attenuator (specifically the V2.0C model from ISR Instrument) in the dB scale to adjust the stimulation amplitudes for each frequency. The attenuated signal was then passed through a custom-designed power amplifier for the purpose of driving a shaker (V101; Ling Dynamic System). A micro-drive stage enabled precise adjustment of the level of static indentation exerted by the shaker along

the z-axis. A plastic contactor with a diameter of 1.9 mm was attached to the shaker to stimulate the skin. Finally, Von Frey hairs were employed to map the receptive field of the area under study. Operations were performed with a Kopf stereotaxic frame and standard surgical instruments. The body temperature was constantly monitored with a rectal thermometer (Physitemp) and was kept stable. A motor-operated surgical drill (Foredom SR), compatible with the Kopf frame, was used to open a craniotomy window by cutting holes in the skull. Throughout the experiment, the subjects' brains were carefully observed and monitored using a surgical microscope (Leica). The entire experiment was performed on a floating table surrounded by a Faraday cage.

The electrodes utilized in the study are manufactured by NeuroNexus Technologies and possess the following dimensions: width: 1.8-mm, length: 1.97-mm, contact diameter: 200 μm, the inter-electrode distance: 500 μm. The electrodes employed in this study are equipped with 16 channels and are designed to record surface potentials from the cortex. They consist of platinum contacts that are securely attached to a polyimide substrate. The potentials recorded during the experiment were first passed through a wide-band head stage and amplified in the LFP band (1-pole lowcut at 0.7 Hz and 1-pole high-cut at 300 Hz) with an amplification of 1000x (Plexon PBX). An oscilloscope (Hitachi) was used to monitor the traces of the evoked responses in each electrode channel. The output signal was transferred to MATLAB for storage after digitization by the USB6251 DAQ card (National Instruments), which was connected in parallel to the circuit.

3.3 Surgery

The subject was weighed to calculate the appropriate dosage of anesthetic cocktail administration. A mixture contained a set quantity of xylazine (10 mg/kg), but the amount of ketamine was adjusted based on the animals' gender and weight (ranging from 60-100 mg/kg). At the start of the experiment, each animal received the full dose of the anesthetic mixture administered intraperitoneally (IP). Throughout the experiment, the palpebral and pedal reflexes of the animals were monitored at regu-

lar intervals, and an additional 1/3 dose was administered when the reflexes began to return. After confirming that the animal was under surgical anesthesia by checking reflexes, the area of the skull was shaved using a hair trimmer. Subsequently, the animal was positioned on a heated bed with a rectal thermometer. After placing the animal in the stereotaxic frame, atropine was injected to decrease saliva production. At the end of the experiments, animals were euthanized through the IP administration of thiopental at a dose of 200 mg/kg.

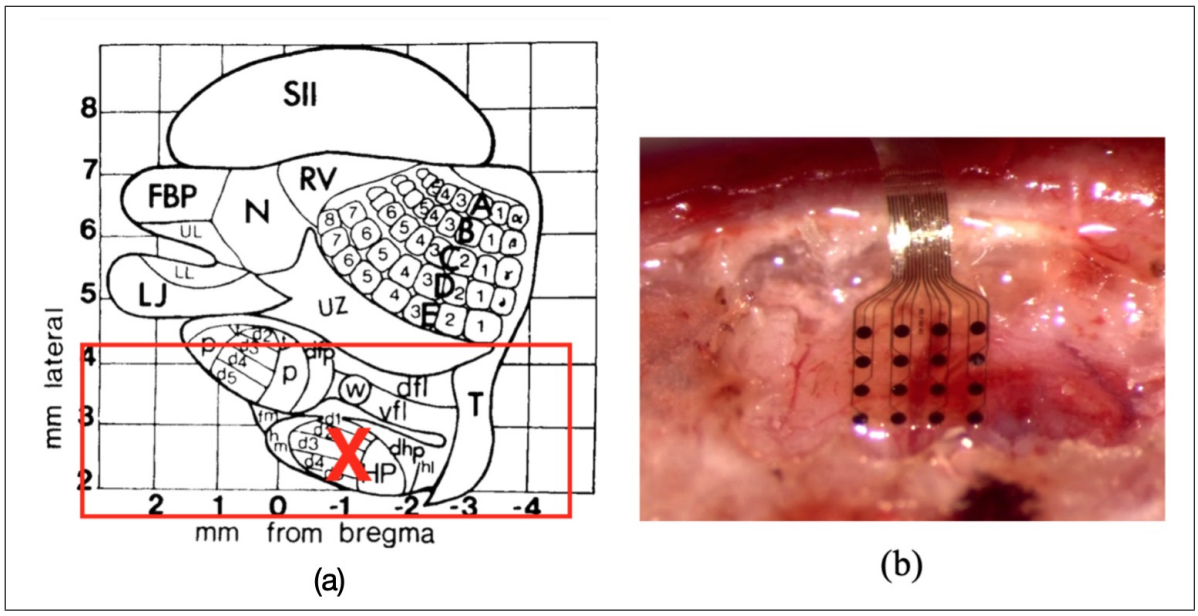

Figure 3.3 Illustration of the craniotomy window targeting the hind paw representation of the somatosensory cortex and the electrode placed on the dura mater. (a) The functional atlas of the rat somatosensory cortex indicates the craniotomy window, demarcated by the red lines, and the approximate hind paw representation, represented by the red cross. Modified from [11]. (b) Placement of the electrode over duramater.

The surgical procedure commenced once the animals' reflexes had completely disappeared and their body temperature had stabilized at approximately $37°C$. Approximately 3 cm incisions were made on the scalp, following the midline. The connective tissues covering the cortex were carefully removed to enhance visibility and stabilize the electrode. Micro hemorrhages resulting from capillary dissection were suppressed using medical sponges. After cleaning the area with saline solution, the corner coordinates of the craniotomy window are identified and marked with a pen. The z-coordinates were adjusted to ensure that the skull was exactly parallel to the horizontal plane. In the left hemisphere, a total of 8 holes were drilled, located in the

middle of each edge and at the corners of the craniotomy window previously marked with a pen. The skull fragment was then delicately detached from the underlying tissue while ensuring the duramater remained intact. The craniotomy window used throughout the experiments is shown in Figure 3.3. Following the completion of the craniotomy, the cortex was rinsed with an artificial cerebrospinal fluid (aCSF) to clean it. Subsequently, any excess fluid was carefully dried to stabilize the electrode.

3.4 Vibrotactile Stimuli and Epidural Field Potentials

In this study, a mechanical sinusoidal vibrotactile stimulus was employed to stimulate the mechanoreceptors of the hind paw. The shaker's probe was positioned to apply 0.5-mm static indentation on the skin, and the mechanical stimulus was applied on top of this indentation. The prior vibrotactile stimulus was administered for a duration of 1 second, followed by the application of the second stimulus (test stimulus) for a duration of 0.5 seconds. Both stimuli were characterized by a rise/fall time of 50 ms at the beginning and end, as depicted in Figure 3.4. Both stimuli were utilized with three distinct frequency values, namely 5 Hz, 40 Hz, and 250 Hz. Another parameter was the temporal gap between the two stimuli. The test stimulus was applied either at 1.16 seconds or 1.36 seconds after the prior stimulus, with the temporal gap ranging between 100 ms and 300 ms, which varied across different experiments. The parameters explained above resulted in 18 conditions (3 prior stimulus frequency * 3 test stimulus frequency * 2 temporal gap), and these conditions were randomly applied in each session. The total duration of each trial was 2 seconds. A 3-second interval was set between successive trials.

Prior and test stimuli were applied at the combination of two different amplitude levels. The attenuation levels of the prior and test stimuli were changed by using the attenuator and were set for each condition based on corresponding frequencies. The prior stimulus was not presented in the first two conditions. Therefore, only the amplitude of the second stimulus was changed. In the next four conditions, there were two stimuli (prior and test).

Table 3.1 shows the corresponding amplitude levels for each stimulation frequency. Attenuation levels were kept the same for both stimuli, and calibration was performed considering the DAC card output. Ten trials for each attenuation level were recorded.

Table 3.1
Conversion table of the corresponding attenuation values to vibrotactile displacement amplitudes (zero to peak).

Attenuation Level	5 Hz (1V)	40 Hz (1V)	250 Hz (10V)
17 dB	210 μm	216 μm	-
14 dB	-	-	209μm
10 dB	464 μm	478 μm	-
7 dB	-	-	465 μm

In Figure 3.4, example waveforms used for mechanical stimulation are presented. The first row shows three test stimuli with 5 Hz, 40 Hz, and 250 Hz, respectively. The second row illustrates the delivery of stimulus pairs with a temporal gap of 100 ms. Specifically, it shows experimental conditions where the prior and test frequencies are 5 Hz (d), 40 Hz (e), and 250 Hz (f), respectively. The last row demonstrates how these stimulus pairs are applied with a temporal gap of 300 ms, 5-5 Hz (g), 40-40 Hz (h), and 250-250 Hz (i), respectively. As previously mentioned, the test stimulus was delivered either 1.16 seconds or 1.36 seconds after the prior stimulus, depending on the varying temporal gap. Note that, in some experimental conditions, the frequencies of the prior and test stimuli were not the same (not shown in Figure 3.4).

The channel exhibiting the highest epidural evoked response to hind paw stimulation using von Frey hairs was identified by looking at the oscilloscope. The hind paw was fixed using modeling clay. As a result, the shaker probe was positioned at the center of the region on the hind paw that exhibited the highest evoked response. The recorded EFPs were initially filtered by the hardware within the frequency range between 0.7 to 300 Hz. There were 16 channels for each electrode, but only 13 of them were used due to input limitations in the recording setup.

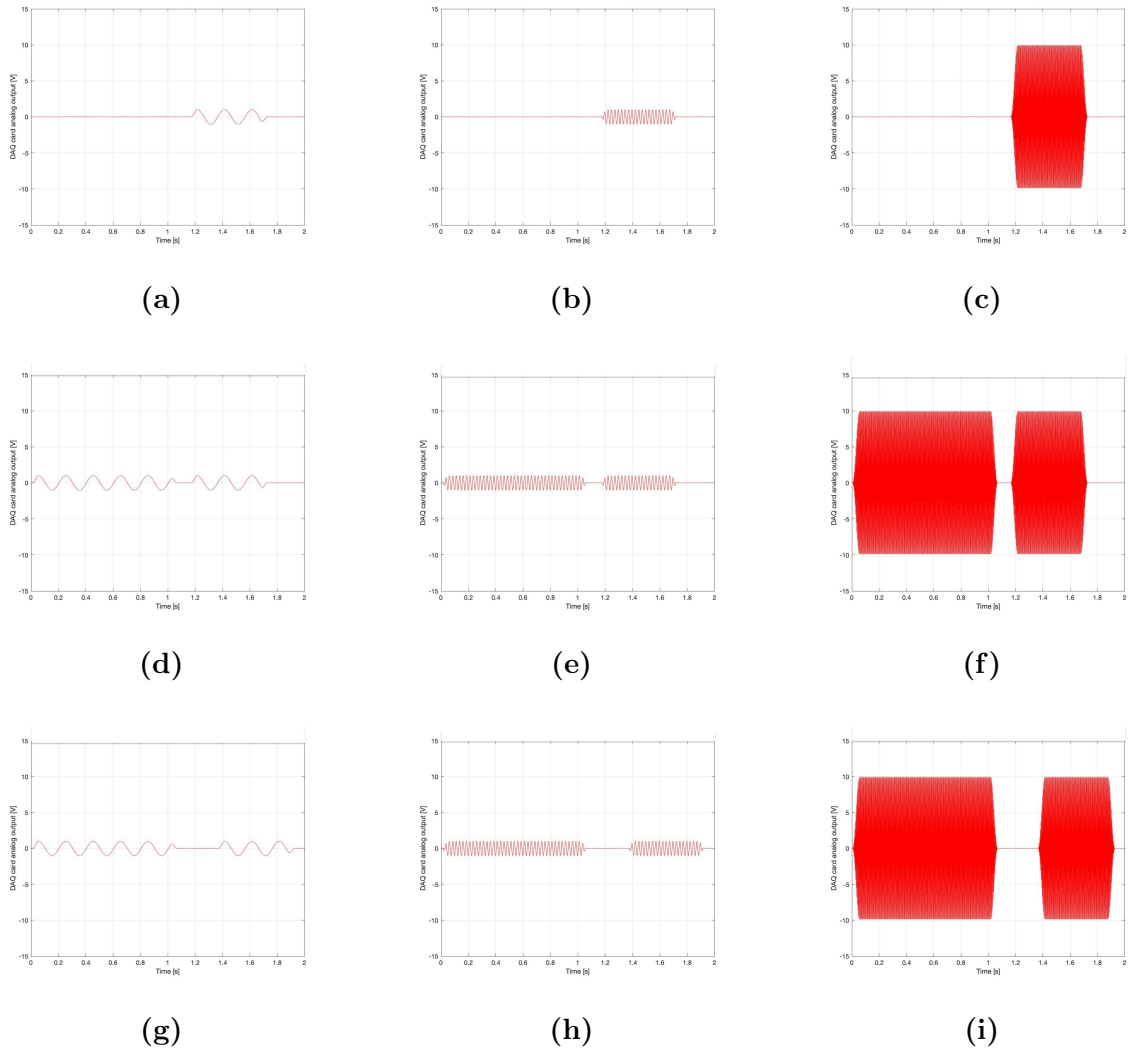

Figure 3.4 The waveforms used for mechanical stimulation. The first row shows the 5 Hz (a), 40 Hz (b), and 250 Hz (c) test stimuli, respectively. An example of experimental conditions with a 100 msec temporal gap is depicted on the 2nd row (d, e, f) and 300 msec on the 3rd row (g, h, i). Note that, in some experimental conditions, the frequencies of the prior and test stimuli were different, not shown in this figure.

3.5 Procedure

The experimental procedure commenced after localizing the shaker and setting up the recording equipment. Each randomized condition, which contained specific prior and test stimulus frequencies along with a particular temporal gap, was applied. As mentioned in the vibrotactile stimuli section, the trial duration was set to 2 seconds, with the first stimulus delivered at the beginning of the trial for 1 second. The second stimulus lasted 0.5 seconds and was delivered after the prior stimulus and specified temporal gap. The inter-stimulus interval was 3 seconds.

The side of stimulation (contralateral or ipsilateral) was randomized in each experiment. The 18 experimental conditions were randomly selected, and approximately 4 minutes of recording were performed for each experimental condition, with varying attenuation levels. Subsequent experimental conditions were applied randomly after the completion of the previous one. The entire experiment for a single subject, including surgery and recording, took approximately 8 hours.

3.6 Data Analysis

For this thesis, only recordings for the contralateral stimulation were analyzed. Following data collection, the analysis was performed using MATLAB. Initially, the data underwent filtering using a 2nd-order zero-phase Butterworth bandpass filter with a range of 4 Hz to 150 Hz. During the analysis, each trial was individually plotted, and trials that had artifacts were identified for exclusion in the subsequent stage of the analysis.

The time average of trials after the artifact exclusion was calculated and plotted at each amplitude level. This trial-averaged analysis allowed for visualizing the tactile evoked responses separately. The color codes depicted in Figure 3.5 represent six distinct conditions, with trial-averaged activity from 10 trials. As mentioned earlier, in the first two rows, only the test stimulus was presented (onset: 1.16 sec). The first trace is for the test stimulus at the higher amplitude level (465 μm), while the second trace is for the test stimulus at the lower amplitude level (209μm). The remaining rows contained traces for different combinations of prior and test stimulus levels. Specifically, the 3rd and 4th traces are for the high-level prior stimulus (478 μm). 5th and 6th traces are for the low-level prior stimulus (216μm). The prior stimulus starts at 0 seconds and has a duration of 1 second.

Two distinct time windows were established for each trial averaged trace to assess changes in EFPs at the onset time window. The time windows are presented in Figure 3.5 as follows;

- Tb (baseline window): The baseline window was defined as the period of 0.1 seconds preceding the presentation of the test stimulus.
- To (Onset window): The analysis window was defined as the first 0.15 seconds following the test stimulus onset.

Specifically, when the temporal gap was set to 100 milliseconds, the test stimulus began at 1.16 seconds. When the temporal gap was set to 300 milliseconds, the test stimulus began at 1.36 seconds. The test stimulus had an approximate duration of 0.56 seconds, taking into account the rise and fall times (cosine squared envelope) of the stimulus (0.06 sec).

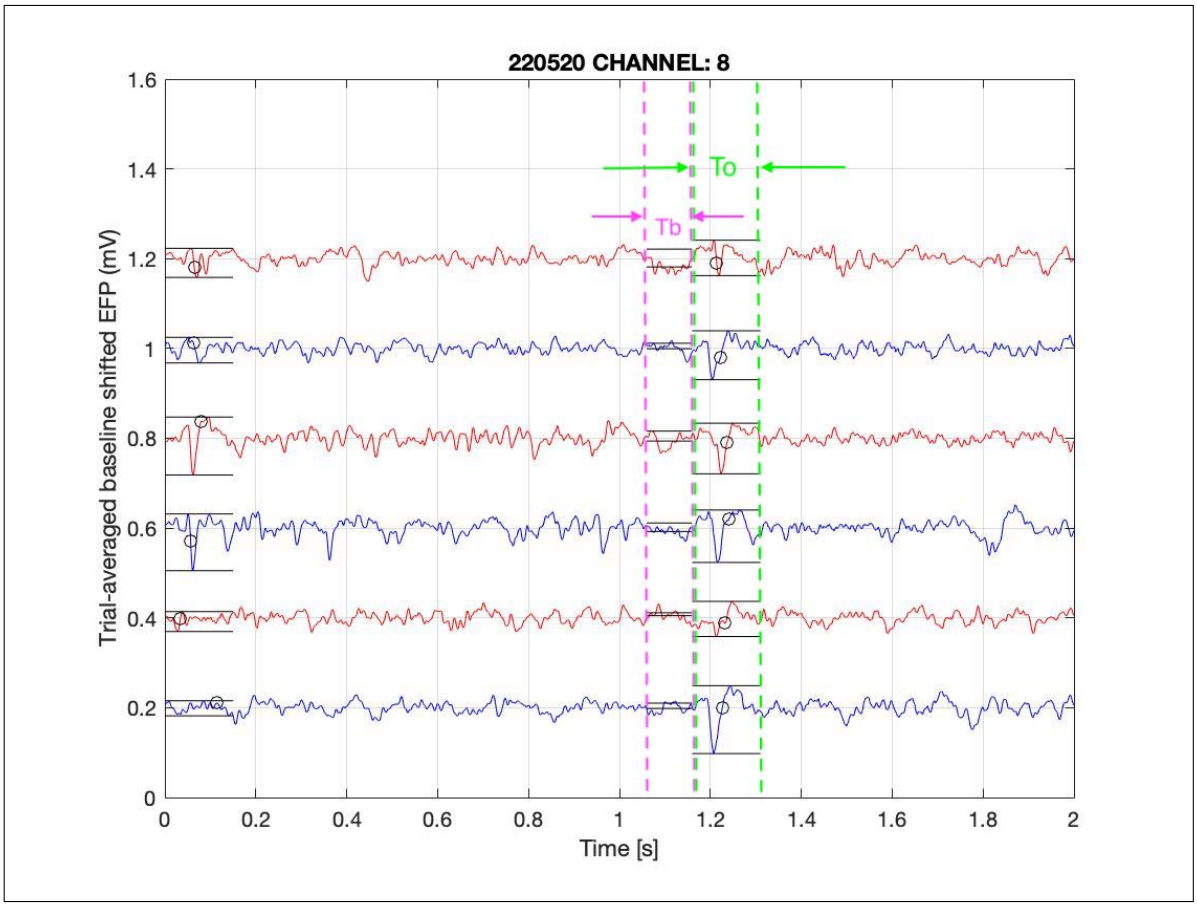

Figure 3.5 Anaysis windows are depicted. Traces are baseline shifted for plotting purposes. Tb: Baseline, To: Onset period.

For the onset analysis of trial-averaged EFPs, only the onset period (To) during

the test stimulus was examined, as shown above. We extracted the following parameters from the trial-averaged EFPs for all subjects (17 rats), experiment conditions (18 frequency and temporal gap combinations), amplitude conditions (6 attenuation level combinations), and recording channels (13 electrode contacts).

Initially, the RMS value for the baseline time window (Tb) was computed using Eq. 3.1; the variable x represents the window of interest, N represents the sample number within that window, and V_n denotes the value of the voltage at a specific time point.

$$V_{RMSx} = \sqrt{\frac{1}{N}\sum_{n=1}^{N}|V_n|^2} \tag{3.1}$$

Next, the amplitude of the EFP in the onset time window (To) was calculated by subtracting the minimum value from the maximum value ($A_{peak-to-peak}$). Subsequently, the latencies were determined by averaging the time indices of the maximum and minimum values within the onset window and dividing the result by the sampling frequency. In Figure 3.5, the baseline time window and maximum and minimum values in the onset window are depicted using straight lines, while the latencies are indicated by black circles for visual clarity.

Following the computation of the peak-to-peak amplitudes ($A_{peak-to-peak}$) within the onset window, these values were divided by the baseline RMS values ($V_{RMSbaseline}$) to obtain a signal-to-baseline (SBRs) measure for vibrotactile response as shown in Eq. 3.2.

$$SBR = \frac{A_{peak-to-peak}}{V_{RMSbaseline}} \tag{3.2}$$

A response criterion was established to determine which data will be subjected to further analysis. In brief, $A_{peak-to-peak}$ was expected to be %10 more than the

$V_{RMSbaseline} \times 6$.

Initially, the highest SBR was found among the channels for each experimental condition and amplitude condition. For each subject, the channel which gave the highest SBR was selected for the traces of the highest test stimulus level without the prior stimulus. If this SBR from the selected channel satisfies the vibrotactile response criterion, the following measures were calculated.

The dB difference (log base 10) was computed to study the effect of the prior stimulus on the vibrotactile response of the test stimulus. For each prior and test attenuation combination, the dB difference was calculated with E.q 3.3 ;

$$20 \times \log 10(\frac{SBR_{with\,prior}}{SBR_{without\,prior}}) \tag{3.3}$$

Additionally, the latency difference was calculated by subtracting the latency for without prior conditions from the latency for with prior conditions with equation 3.4;

$$latency_{with\,prior} - latency_{without\,prior} \tag{3.4}$$

The channel with the highest SBR was also analyzed for the traces when a weaker test stimulus was applied without the prior stimulus. If the EFP satisfied the vibrotactile response criterion, similar measures to analyze the effects of the prior stimulus were calculated.

In summary, the dB and latency differences, along with their corresponding frequency and amplitude conditions, were saved for statistical analysis. Notably, a negative dB difference indicated the suppressive effect of the prior stimulus on the test stimulus, whereas a positive dB difference indicated the facilitating effect. Similarly, a positive latency difference indicated the vibrotactile response was delayed because of the prior stimulus, whereas a negative latency difference indicated the opposite. Before statistical analysis, these measures were analyzed for outliers using Peirce's Criterion method, which is one of the most rigorous methods known for the outlier analysis [80].

To conduct statistical analysis on dB and latency differences, random intercept linear mixed-effects models (LMMs) were employed via SPSS Version 27 (IBM). The model analyzed the measures described above, including the frequency of the prior stimulus and the test stimulus, the temporal gap, the amplitude of the prior stimulus, and the test stimulus as the fixed factors (independent variables). All independent variables were at the ordinal scale in the model.

Eq. 3.5 describes the mathematical function of the LMM model utilized for the analysis. In the model, β's are the regression coefficients, E is the frequency of the prior stimulus (fixed effect), S is the frequency of the test stimulus (fixed effect), F is the temporal gap (fixed effect), D is the amplitude of the prior frequency (fixed effect), T is the amplitude of the test frequency (fixed effect), u_i is the random intercept due to subjects, ϵ_{ijklmn} is the residual error and y_{ijklmn} is the dependent variable (latency difference or dB difference).

$$y_{ijklmn} = \beta_0 + \beta_1 E_j + \beta_2 S_k + \beta_3 F_l + \beta_4 D_m + \beta_5 T_n + interactions + u_i + \varepsilon_i jklmn \quad (3.5)$$

4. RESULTS

4.1 Qualitative Description of the Recorded Traces

The collected data were first analyzed by visually inspecting the recorded traces, which enabled the investigation of their qualitative characteristics. As previously mentioned, only recordings from the contralateral hemisphere were analyzed. Each plot displayed the stimulation waveforms and the corresponding recorded neural activity to demonstrate the temporal synchronization between neural activity in the onset window and delivery of the stimulus. It is important to note that only the arbitrary number of stimulation waveforms was plotted.

For each frequency (5Hz, 40Hz, 250Hz), ten trials were recorded at different amplitude levels (for 5 Hz: 210-464 μm, for 40 Hz: 216-478 μm, for 250 Hz: 209-465 μm). Two attenuation levels were used for each test stimulus and the prior stimulus. Therefore, a total of 60 trials were recorded for six different conditions. The first two conditions (20 trials) only had the test stimulus, while the remaining four had both the prior and test stimuli. It was expected that the highest response would be observed in the first condition where there was no prior stimulus and the amplitude of the test stimulus was the highest. The recorded trials were primarily examined through visual inspection (see Figure 4.1).

Figure 4.1 (a) illustrates the plotted experimental condition in which a prior stimulus of 5 Hz is followed by a test stimulus, also of 5 Hz, separated by a temporal gap of 100 milliseconds (msec). The duration of the prior stimulus is 1 second, while the test stimulus lasts for 0.5 seconds, delivered at 1.16 seconds with a 100 msec temporal gap. This sequence is visualized at the top of the plot with stimulus traces. During plotting this group of traces, conditions of varying amplitude levels were assigned color codes: blue and red. When analyzing the plot from the bottom to the top, only a high amplitude test stimulus was applied in the first ten trials, coded in blue. In the

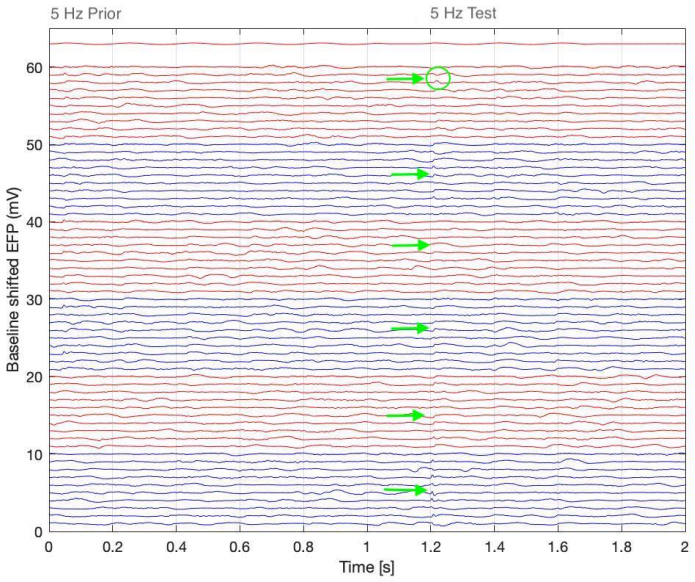

(a)

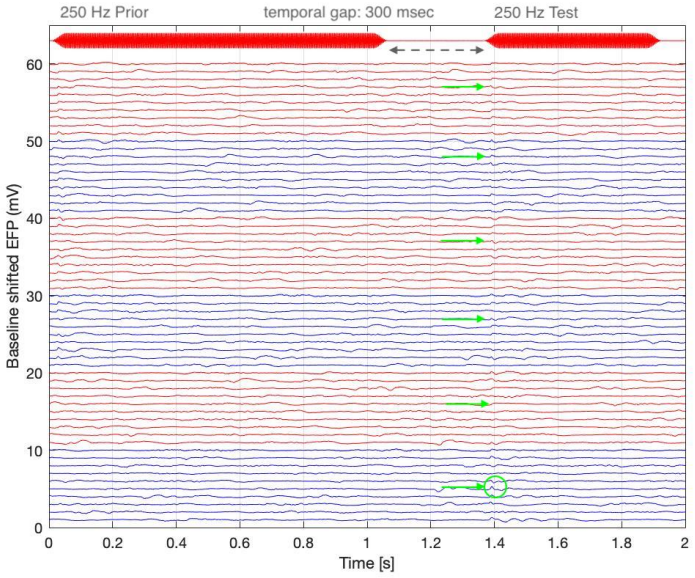

(b)

Figure 4.1 Plots from trial by trial analysis of Tactile Evoked Potentials from experiment 220408. The variation in colors denotes different conditions representing different amplitude levels for each frequency pair; the first row of each figure represents the conditions where only the test stimulus was presented with the highest amplitude. The next four rows (3-6) represent the conditions where the prior and test stimuli were presented, with varying amplitude levels for each. Traces recorded from Ch-1 for (a) 5-5 Hz with a 100 msec temporal gap, (b) 250-250 Hz with a 300 msec temporal gap.

following ten trials, marked in red, only a low-amplitude test stimulus was applied. In the third trace, both the prior and test stimuli exhibited high amplitude. The fourth trace showed a high amplitude prior stimulus followed by a low amplitude test

stimulus. The fifth trace demonstrates a low-amplitude prior stimulus followed by a high-amplitude test stimulus, and in the sixth trace, both the prior and test stimuli are of low amplitude. Each trace reveals the presence of epidural field potentials at the initiation of the test stimulus, denoted by green arrows. However, the analysis was not extended to the epidural field potentials generated by the prior stimulus.

The trial-by-trial depiction, illustrated in Figure 4.1(b), is plotted for a differing experimental condition. In this experiment, the prior and test stimuli were at 250 Hz, with a temporal gap of 300 milliseconds (msec). The 250 Hz test stimulus was delivered at 1.36 seconds due to the temporal gap of 300 milliseconds. Similar to the previous experiment, trials of varying amplitude levels are color-coded, namely; blue and red. The onset of the test stimulus is accompanied by the epidural field potentials, which are indicated by green lines.

In addition to trial-by-trial analysis, trials corresponding to a specific stimulation frequency and amplitude condition were averaged in time, and the resulting tactile evoked EFPs were plotted. This time-averaging technique was employed to highlight the evoked response that is time-locked to the stimulus by minimizing the effects of noise and unsynchronised activity. Figure 4.2 shows the average EFPs in response to contralateral stimulation. Six different experimental conditions were plotted. In all plots, EFPs are visible at the onset of the test stimulus. Specifically, Figure 4.2(a) and (b) display experimental conditions where the test and prior stimulus are at 5 Hz with a temporal gap of 100 milliseconds in (a) and 300 milliseconds in (b). The tactile-evoked EFPs that form at the onset of the 5 Hz test stimulus are observable for the 500 milliseconds stimulation period. In contrast, Figures 4.2(e) and (f) show conditions where the prior and test stimulus is at 250 Hz. Here, the evoked activity is selected solely within the onset time window, demonstrating a distinction in the behavior of EFPs with different frequencies of the test stimuli.

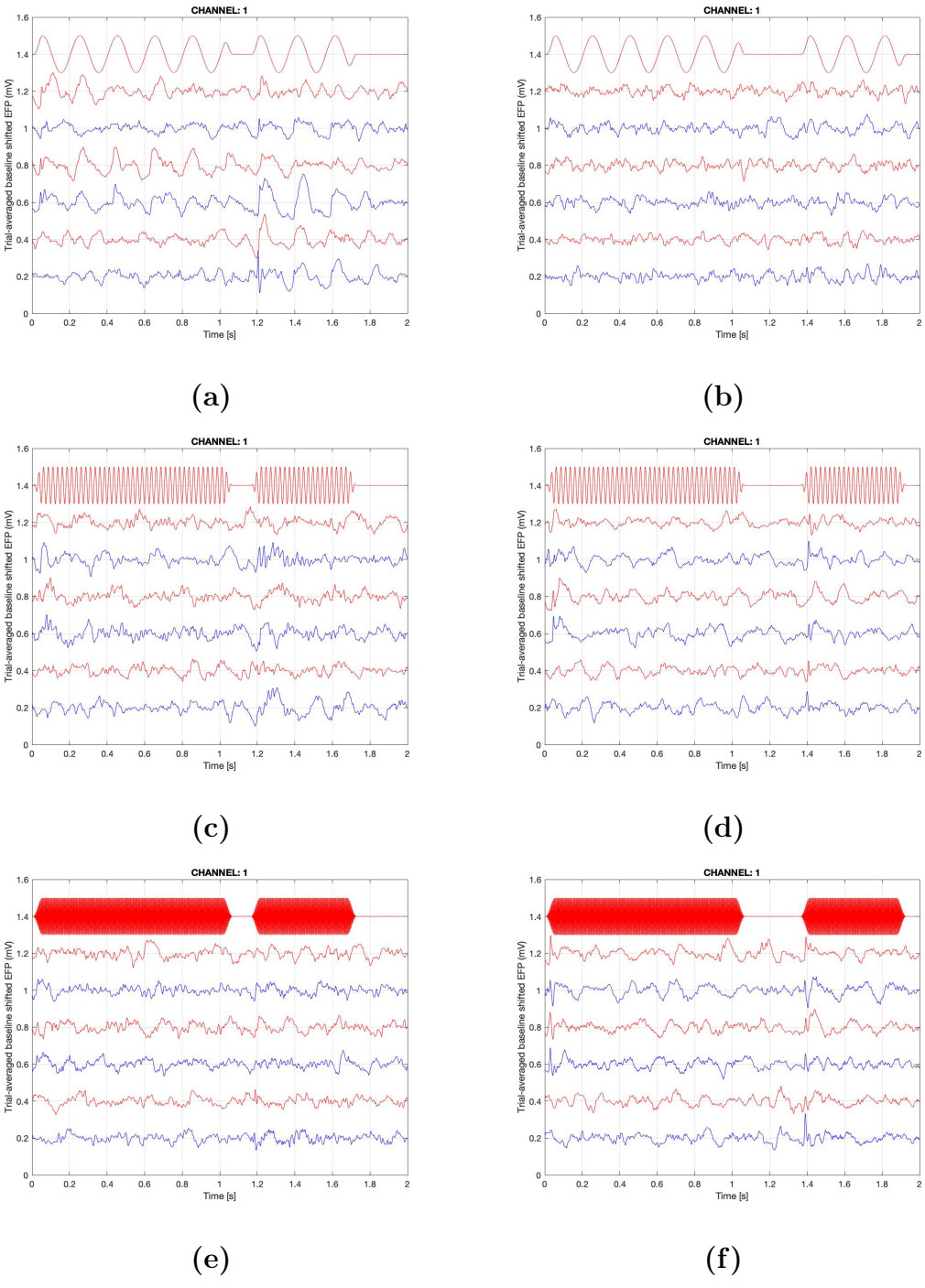

Figure 4.2 Time-averaged Epidural Field potentials were plotted from experiment 220408. Only experiments with prior and test stimulus pairs having the same frequency value were plotted. In (a), (c), and (e) the temporal gap is 100 milliseconds between the stimulus pairs, while in (b), (d), and (f) the temporal gap is 300 milliseconds between stimuli.

4.2 Tactile Evoked Epidural Field Potentials

As outlined in the methodology section, only the channel that met the response criteria and exhibited the highest evoked potential value was considered for further

analysis in each dataset. The dependent variables were the dB difference and latency difference due to prior stimulation. The frequency of the prior stimulus and the test stimulus (5-, 40- and 250-Hz), the temporal gap (100 - 300 msec), the amplitude of the prior stimulus, and the test stimulus were chosen as fixed factors, and the covariate was defined as the subject in the analysis.

4.2.1 Epidural Field Potential Amplitude Changes Due to Prior Stimulation

The effect of the prior stimulus on the dB difference of the test stimulus was predominantly negative across all experiments and conditions. This indicates that the response elicited by the test stimulus was generally suppressed by the prior stimulus. Generally, a greater degree of suppression was observed in the experimental conditions where the temporal gap was 100 milliseconds. This suppression effect is particularly prominent when the frequency of the prior stimulus is 5 Hz. The influence of the temporal gap is shown in Figure 4.3.

Likewise, in experimental conditions where the frequency of the prior stimulus was at 40 Hz, overall, the suppression effect of the prior stimulus tended to decrease as the temporal gap increased (see Figure 4.4). The greatest level of suppression was observed when the frequency of the test stimulus was at 5 Hz. Finally, experimental conditions with a prior stimulus frequency of 250 Hz are shown in Figure 4.5. In particular, the highest suppression was observed when the test stimulus frequency was 5 Hz.

Based on the analysis results, it was found that all fixed factors had a statistically significant effect on the dB difference. The random intercept, which shows potential variability among subjects, was not found to be statistically significant in this analysis($p = 0.069$). The frequency of the prior stimulus was found to be a significant predictor of the dB difference ($F(2, 667.938) = 7.122$, $p < 0.001$).

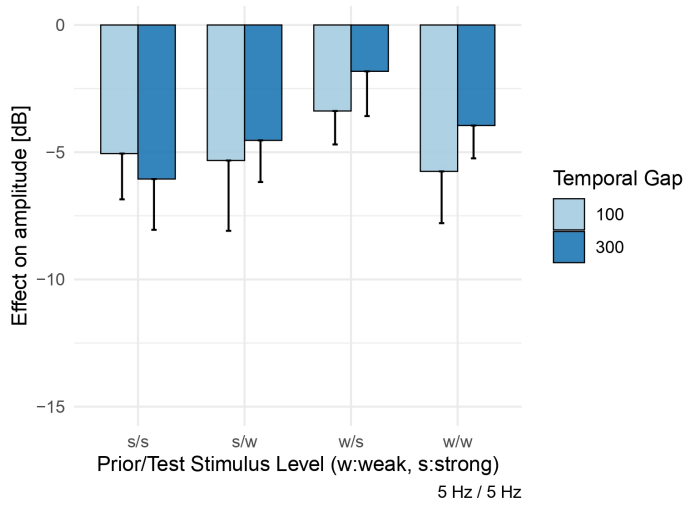

(a)

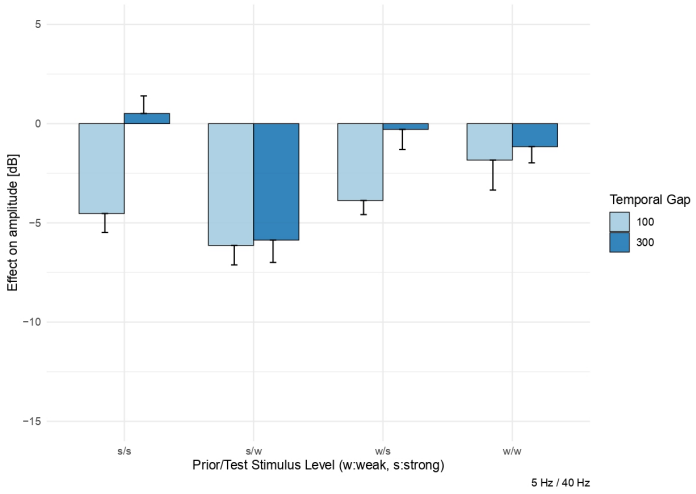

(b)

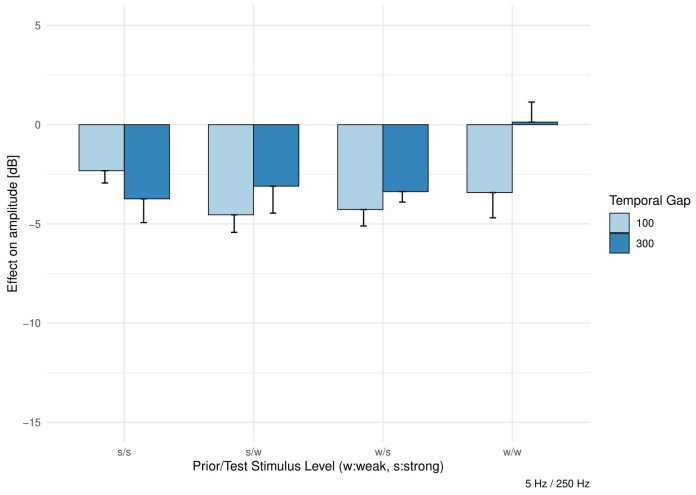

(c)

Figure 4.3 The effect of the temporal gap on the dB difference. The results are shown for a 5 Hz prior stimulus frequency and test stimulus frequencies of 5 Hz (a), 40 Hz (b), and 250 Hz (c), with temporal gaps of 100 msec and 300 msec (color code: light blue for 100 msec and dark blue for 300 msec). The standard error of the mean (SEM) is shown by error bars.

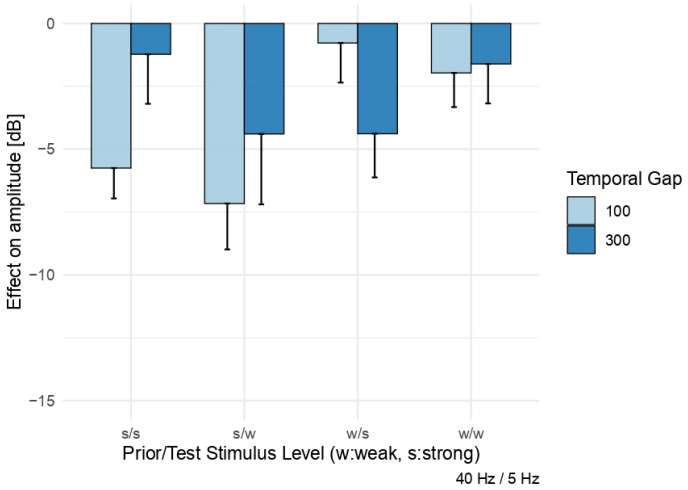

(a)

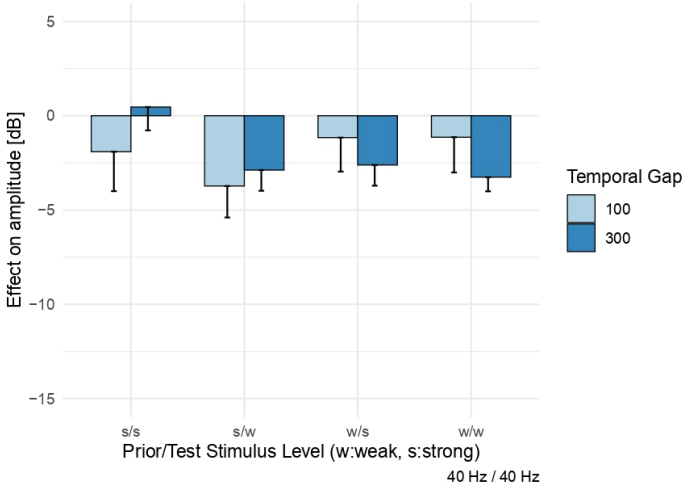

(b)

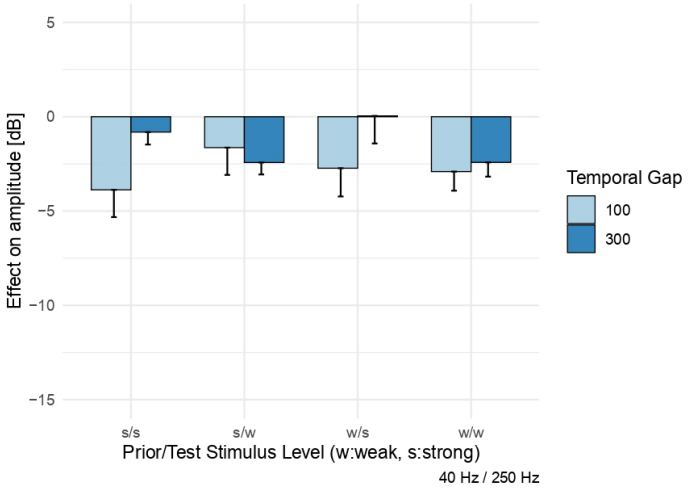

(c)

Figure 4.4 The results are shown for a 40 Hz prior stimulus frequency and test stimulus frequencies of 5 Hz (a), 40 Hz (b), and 250 Hz (c), with temporal gaps of 100 msec and 300 msec (color code: light blue for 100 msec and dark blue for 300 msec).

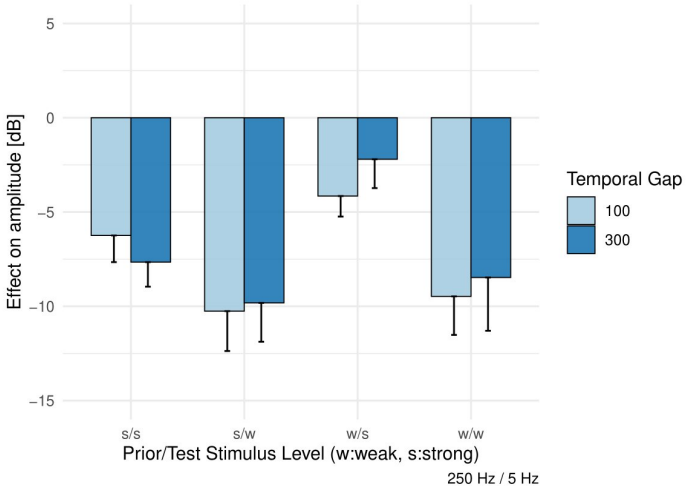

(a)

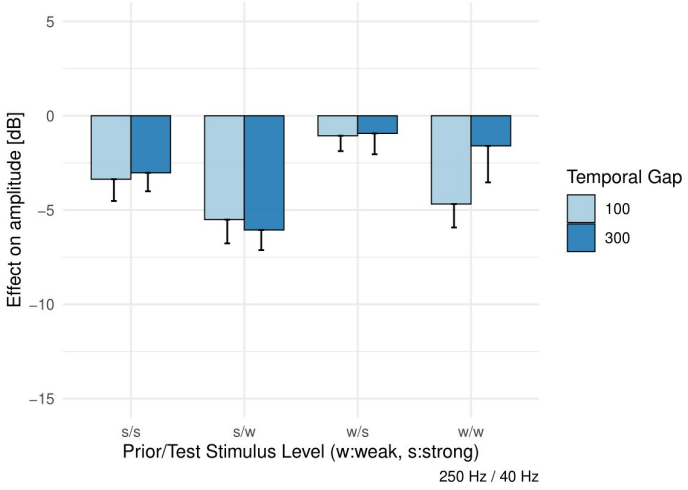

(b)

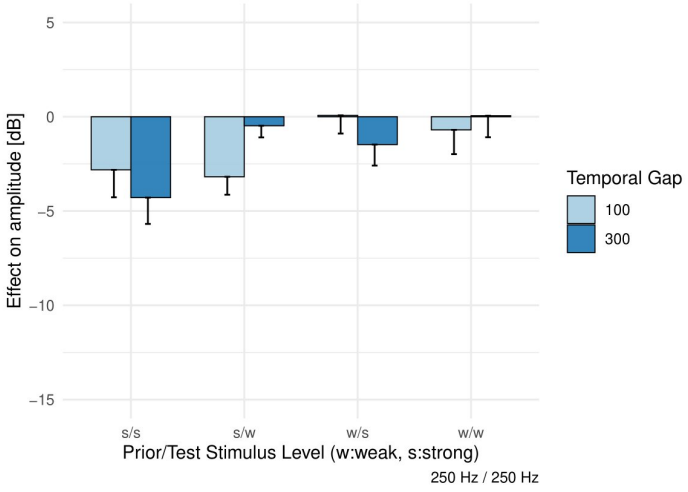

(c)

Figure 4.5 The results are shown for a 250 Hz prior stimulus frequency and test stimulus frequencies of 5 Hz (a), 40 Hz (b), and 250 Hz (c), with temporal gaps of 100 msec and 300 msec (color code: light blue for 100 msec and dark blue for 300 msec).

Based on the mean results, the suppression effect of the prior stimulus on the dB difference was found to be the highest when the prior frequency was 250 Hz (-4.091 ± 0.599). In contrast, it was the lowest when the prior frequency was 40 Hz (-2.574 ± 0.391). This difference was statistically significant(SE = 0.410, df = 665.636, p* < .001). The obtained result has been adjusted using the Bonferroni correction. Notably, regardless of their frequency, all prior stimuli resulted in negative decibel (dB) differences, implying a consistent suppressive effect.

Similarly, the frequency of the test stimulus had a significant impact on the dB difference (F(2, 666.305) = 26.231, p <.001). Mean values showed that the EFP amplitude suppression was the lowest when the test frequency was 250 Hz ($-2.323 \pm .392$). In contrast, it was the highest when the test frequency was 5 Hz ($-5.140 \pm .394$). According to the pairwise comparison results, the effects of most of the test frequencies on the dB difference were found to be statistically significant. Specifically, the difference between the dB difference of 5 Hz and 40 Hz (SE = .410, df = 667.752, p* < .001). , and the difference between the dB difference of 5 Hz and 250 Hz (SE = .419, df = 667.067, p* < .001) was significant. However, the effect of 40 Hz and 250 Hz test stimulus on the dB difference was not statistically significant (SE = 0.449, df = 664.111, p = .810).

Additionally, the temporal gap between the stimuli was strongly associated with the dB difference (F(1, 666.747) = 6.725, p < .01). The dB difference was the highest when the temporal gap was 100 msec (-3.848 ± 0.347). In contrast, it was the lowest when the temporal gap was 300 msec (-2.976 ± 0.356). The trend, depicted in Figure 4.3, is evident for cases where the prior stimulus frequency was 5 Hz.

The amplitude of the prior stimulus (F(1, 662.229) = 21.801, p <.001) and test stimulus (F(1, 668.183) = 11.690, p < .001) were also significant predictors of the dB difference. The absolute dB difference was found to be higher when the prior stimulus had a higher amplitude ($-4.195 \pm .351$), while it was the lowest when the amplitude of the prior stimulus was lower ($-2.629 \pm .351$). On the other hand, the absolute dB difference was found to be higher when the test stimulus had a lower amplitude ($-3.988 \pm .365$), while it was the lowest when the amplitude of the test stimulus was

lower ($-2.835 \pm .338$).

In addition to the significant effects of the fixed factors, certain interactions between some factors were also found to be statistically significant. Specifically, certain combinations of the prior and test stimulus frequencies led to a significant difference in the dB difference compared to other combinations ($F(4, 668.647) = 6.213$, $p < .001$). As shown in Table 4.1, applying a 250 Hz prior and a 5 Hz test stimulus together resulted in the highest suppression ($-7.391 \pm .599$). The lowest suppression was observed when the prior and test stimulus frequency was 250 Hz ($-1.583 \pm .578$).

Table 4.1
Mean dB difference and standard error of conditions for each frequency pair found by the linear mixed-effects model.

Priorfreq (Hz)	Testfreq (Hz)	Mean (dB difference)	Std. Error	df	95% Confidence Interval	
					Lower Bound	Upper Bound
5	5	-4.573	.553	137.300	-5.666	-3.479
	40	-2.924	.580	151.100	-4.071	-1.778
	250	-3.214	.584	152.118	-4.368	-2.060
40	5	-3.456	.580	148.398	-4.603	-2.310
	40	-2.093	.541	121.406	-3.164	-1.022
	250	-2.172	.555	133.402	-3.270	-1.074
250	5	-7.391	.599	169.296	-8.573	-6.209
	40	-3.300	.535	118.869	-4.359	-2.241
	250	-1.583	.578	154.167	-2.726	-.441

Another significant interaction was observed between the frequency and amplitude level of the test stimulus ($F(2, 665.511) = 5.000$, $p < .007$). Table 4.2 demonstrates that, in general, increasing the frequency of the test stimulus reduced suppression regardless of the amplitude. However, the only exception to this trend was observed when the test stimulus had a higher amplitude. Specifically, the 5 Hz low amplitude test stimulus resulted in a greater suppression effect ($-6.130 \pm .521$), whereas the 40 Hz high amplitude test stimulus resulted in the lowest suppression effect ($-1.854 \pm .454$).

The statistical analysis revealed only one significant three-way interaction, which is between the temporal gap and frequency and amplitude of the prior stimulus ($F(2,$

662.291) = 3.664, p <.026). According to the results, the highest absolute dB difference value ($-5.312 \pm .669$) was observed when a 250 Hz prior stimulus with a higher amplitude was presented with a 300 msec temporal gap, as shown in Table 4.3. Conversely, the lowest absolute dB difference was observed when a low amplitude 5 Hz prior stimulus was presented with a 300 msec temporal gap ($-1.856 \pm .641$).

Table 4.2
mean and standard error of the interaction between frequency and amplitude of the test stimulus.

Testfreq (Hz)	Testamp (μm)	Mean (dB difference)	Std. Error	df	95% Confidence Interval	
					Lower Bound	Upper Bound
5	210 μm	-6.130	.521	109.059	-7.162	-5.098
	464 μm	-4.150	.465	71.566	-5.077	-3.223
40	216 μm	-3.691	.495	87.135	-4.674	-2.707
	478 μm	-1.854	.454	65.455	-2.761	-.947
250	209μm	-2.144	.520	103.032	-3.176	-1.113
	465 μm	-2.502	.460	68.515	-3.419	-1.584

Table 4.3
The mean and standard error of the interaction between amplitude and frequency of the prior stimulus and temporal gap.

Priorfreq (Hz)	Tempgap (msec)	Prioramp (μm)	Mean (dB difference)	Std. Error	df	95% Confidence Interval	
						Lower Bound	Upper Bound
5	100	210 μm	-3.797	.644	223.54	-5.066	-2.527
		464 μm	-4.745	.646	225.021	-6.017	-3.472
	300	210 μm	-1.856	.641	207.042	-3.120	-.593
		464 μm	-3.885	.639	204.954	-5.144	-2.625
40	100	216 μm	-1.863	.623	192.368	-3.091	-.635
		478 μm	-4.129	.614	183.382	-5.340	-2.918
	300	216 μm	-2.421	.625	194.715	-3.653	-1.189
		478 μm	-1.882	.645	217.224	-3.154	-.611
250	100	209μm	-3.338	.618	192.612	-4.557	-2.119
		465 μm	-5.217	.611	186.607	-6.422	-4.013
	300	209μm	-2.498	.667	238.131	-3.812	-1.183
		465 μm	-5.312	.669	239.129	-6.630	-3.994

4.2.2 Epidural Field Potential Latency Changes Due to Prior Stimulation

The effect of the prior stimulus on the latency of the test stimulus was shown for all experimental conditions. The impact of the prior stimulus on the latency difference of the test stimulus was largely positive. This finding indicates a delayed evoked response of the test stimulus. In general, the analysis reveals an interesting trend concerning latency differences: as the frequency of the prior stimulus increases, the latency difference also tends to increase. Conversely, as the frequency of the test stimulus increases, the latency difference tends to decrease (see Figure 4.6, 4.7, 4.8).

The study investigated fixed factors' effect on the second dependent variable, namely latency difference. Among the fixed factors, it has been found that the frequency of the prior stimulus ($F(2, 648.597) = 9.815$, $p < 0.001$), the frequency of the test stimulus ($F(2, 647.911) = 11.517$, $p < 0.001$) and the amplitude of the test stimulus ($F(1, 654.005) = 7.129$, $p < 0.008$) have statistically significant effects on the latency difference. However, the effects of the amplitude of the prior stimulus ($F(1, 637.472) = 1.599$, $p = 0.207$) and the temporal gap ($F(1, 648.135) = 0.047$, $p = 0.829$) on latency difference were not statistically significant. Furthermore, according to the analysis results, the subject effect, represented as the intercept in the model, did not have a significant influence on the latency difference ($p = 0.353$).

Based on the mean results, the latency difference was the lowest when the prior frequency was 5 Hz ($.001 \pm .002$) and the highest when the prior frequency was 250 Hz ($.009 \pm .002$). Notably, positive latency values indicate a delay in the tactile-evoked epidural field potentials. According to the pairwise comparison results, the difference between 5 Hz and 250 Hz ($p^* < .001$) and 40 Hz and 250 Hz ($p^* < .005$) were statistically significant. However, the difference between 5 Hz and 40 Hz was not statistically significant ($p = .661$).

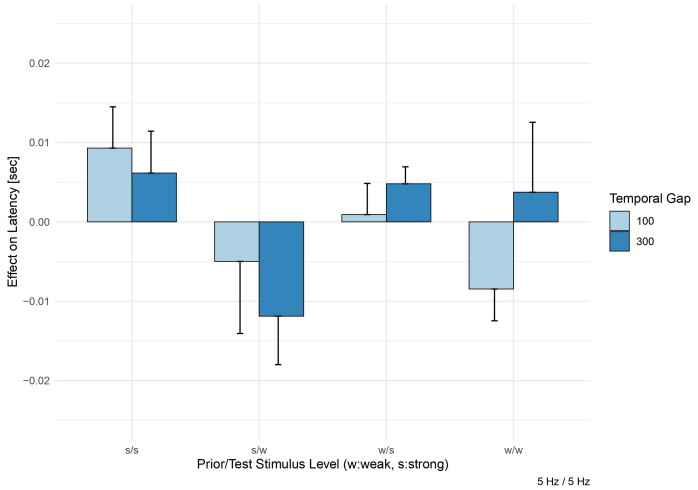

(a)

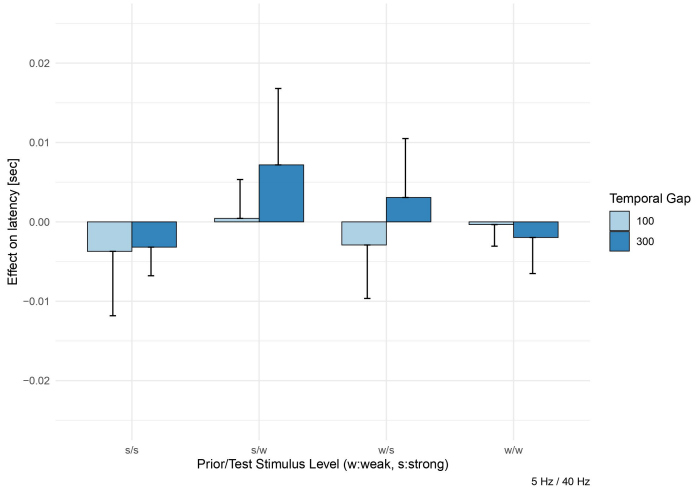

(b)

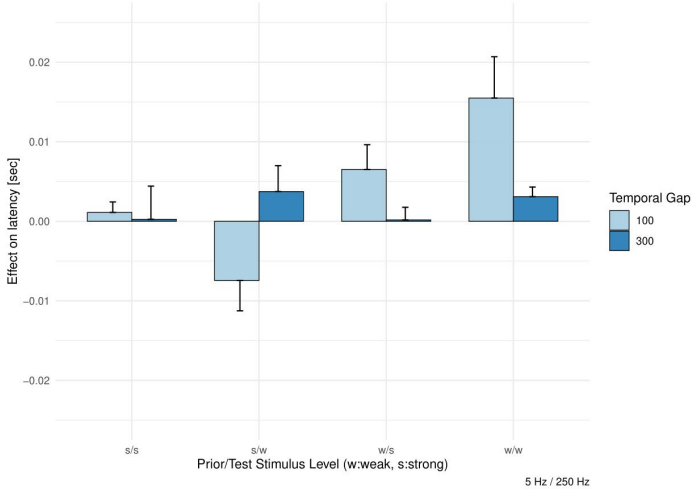

(c)

Figure 4.6 The effect of the prior stimulus on the latency difference. The results are shown for a 5 Hz prior stimulus frequency and test stimulus frequencies of 5 Hz (a), 40 Hz (b), and 250 Hz (c), with temporal gaps of 100 msec and 300 msec (color code: light blue for 100 msec and dark blue for 300 msec). The standard error of the mean (SEM) is shown by error bars.

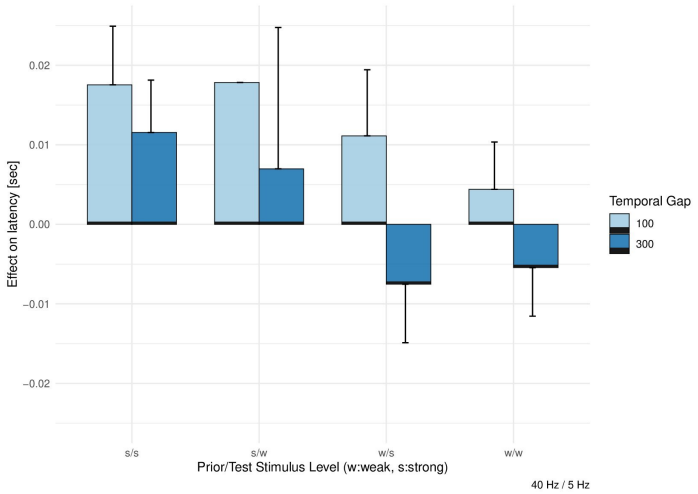

(a)

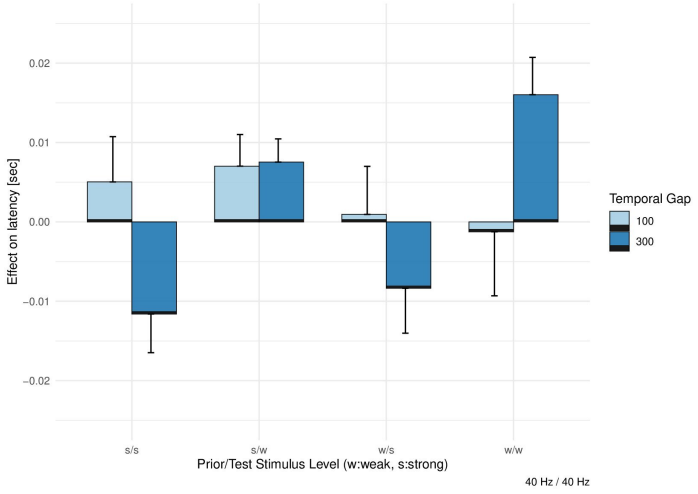

(b)

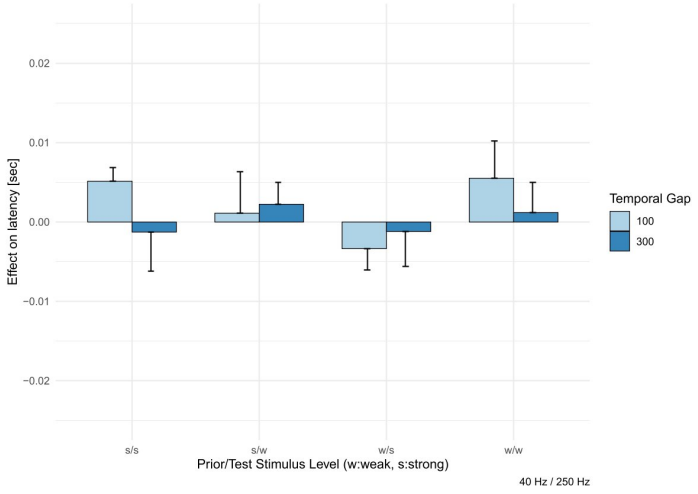

(c)

Figure 4.7 The effect of the prior stimulus on the latency difference. The results are shown for a 40 Hz prior stimulus frequency and test stimulus frequencies of 5 Hz (a), 40 Hz (b), and 250 Hz (c), with temporal gaps of 100 msec and 300 msec (color code: light blue for 100 msec and dark blue for 300 msec). The standard error of the mean (SEM) is shown by error bars.

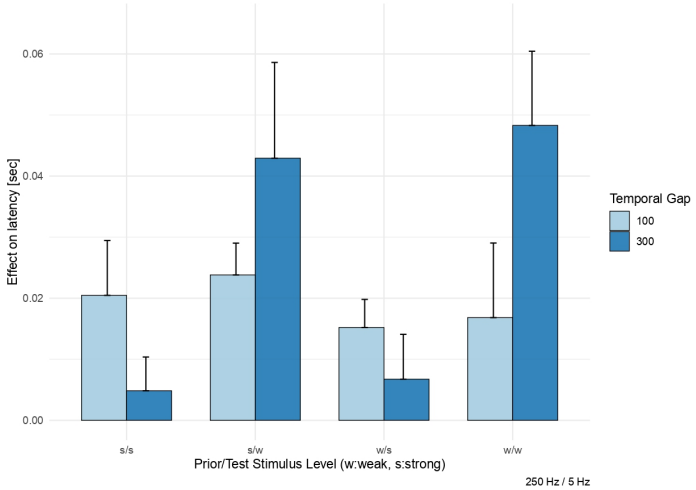

(a)

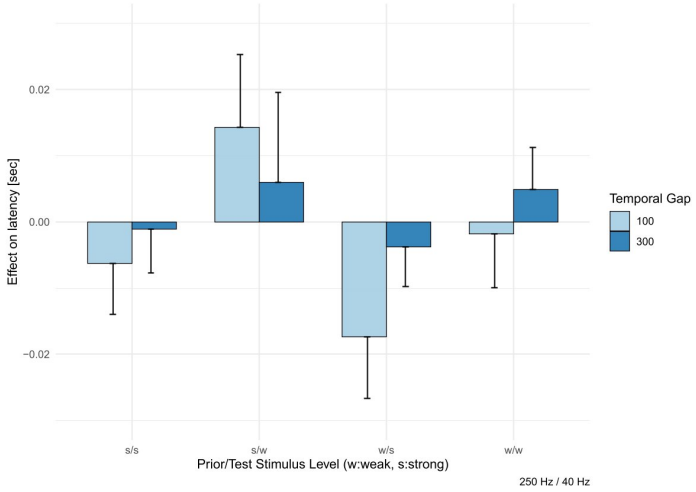

(b)

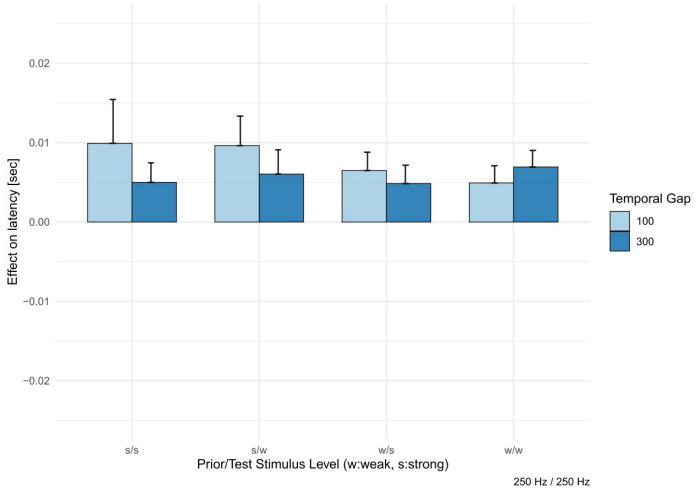

(c)

Figure 4.8 The effect of the prior stimulus on the latency difference. The results are shown for a 250 Hz prior stimulus frequency and test stimulus frequencies of 5 Hz (a), 40 Hz (b), and 250 Hz (c), with temporal gaps of 100 msec and 300 msec (color code: light blue for 100 msec and dark blue for 300 msec). The standard error of the mean (SEM) is shown by error bars.

The effects of test frequency on latency difference were investigated based on mean values and pairwise comparison results. Mean results showed that the latency difference was the least when the test frequency was 40 Hz ($0.0001 \pm .002$). In contrast, it was the highest when the test frequency was 5 Hz ($0.010 \pm .002$). According to the pairwise comparison results, the effects of most of the test frequencies on the latency difference were found to be statistically significant. Specifically, the difference between 5 Hz and 40 Hz ($p^* < .001$) and 5 Hz and 250 Hz ($p^* < .005$) were statistically significant. Whereas the difference between 40 Hz and 250 Hz was not significant ($p = .349$).

Additionally, the effects of test amplitude on latency difference were investigated. Mean results showed that the latency difference was the lowest when the test amplitude was higher ($0.002 \pm .001$). In contrast, it was the highest when the test amplitude was lower ($0.007 \pm .001$). According to the pairwise comparison result, different test amplitude has a significantly different effect on the latency difference ($p^* < .008$).

Similar to the dB difference analysis, the result of the analysis for latency difference revealed certain significant interactions between fixed factors. Specifically, certain combinations of the prior and test stimulus frequencies led to a significant difference in the latency difference compared to other combinations ($F(4, 650.884) = 6.785$, $p < .001$). As shown in Table 4.4, applying a 250 Hz prior and a 5 Hz test stimulus together resulted in the highest latency difference similar to the dB difference ($.022 \pm .003$). The latency difference was found to be the smallest for experiments where the prior stimulus frequency was 250 Hz, and the test stimulus frequency was 40 Hz, with a mean value of ($-.001 \pm .002$). It is important to note that a positive latency value signifies a delay in the evoked response, whereas a negative latency value indicates that the evoked response occurs earlier than expected.

Another important interaction was found between the frequency of the prior stimulus and the test stimulus amplitude $F(2, 650.018) = 5.319$, $p < .005$). The highest latency difference was observed when the 250 Hz prior stimulus was paired with a lower amplitude test stimulus (0.015 ± 0.002), as shown in Table 4.5. The latency difference

was found to be the lowest for experiments where the prior stimulus frequency was 5 Hz, and the amplitude of the test stimulus was lower ($.000 \pm .002$). It should be noted that when the test stimulus amplitude was low; an increase in the frequency of the prior stimulus led to an increase in the latency difference.

Table 4.4
Effect of each frequency pair on latency difference found by the linear mixed-effects model.

Priorfreq (Hz)	Testfreq (Hz)	Mean latency difference (sec)	Std. Error	df	95% Confidence Interval	
					Lower Bound	Upper Bound
5	5	.000	.003	161.400	-.005	.005
	40	.000	.003	164.845	-.005	.005
	250	.002	.003	162.977	-.003	.007
40	5	.007	.003	146.354	.002	.012
	40	.002	.002	140.730	-.003	.007
	250	.001	.002	139.054	-.004	.006
250	5	.022	.003	206.707	.017	.028
	40	-.001	.002	124.657	-.006	.004
	250	.007	.003	173.040	.002	.012

Table 4.5
Effect of the interaction between the prior stimulus' frequency and test stimulus' amplitude on latency difference.

Priorfreq (Hz)	Testamp (μm)	Mean latency difference (sec)	Std. Error	df	95% Confidence Interval	
					Lower Bound	Upper Bound
5	210 μm	.000	.002	107.467	-.005	.004
	464 μm	.002	.002	70.047	-.002	.006
40	216 μm	.005	.002	82.768	.001	.009
	478 μm	.001	.002	69.809	-.003	.005
250	209μm	.015	.002	113.301	.010	.019
	465 μm	.004	.002	64.966	-5.950E-5	.008

Finally, the last significant 2-way interaction was found between the temporal gap and the amplitude of the test stimulus $F(1, 643.218) = 3.877$, $p < .049$). The highest latency difference was found when the temporal gap was 300 msec, and the test stimulus amplitude was low (0.008 ± 0.002). Conversely, the lowest latency difference was observed when the temporal gap was 300 msec, and the test stimulus amplitude was high (0.001 ± 0.002). The analysis also identified two significant multiple interactions. The first one was between the frequency of the prior stimulus, the frequency of the test stimulus, and the amplitude of the test stimulus $F(4, 646.980) = 3.159$, $p < .014$).

The second significant interaction was between the frequency of the prior stimulus, the frequency of the test stimulus, the temporal gap, and the amplitude of the test stimulus $F(4, 644.805) = 3.397$, $p < .009$).

5. DISCUSSION

The effects of prior stimulation on tactile evoked epidural field potentials in rat S1 cortex were investigated. This was achieved by analysis of epidural field potentials recorded from the cortical surface by 16-channel ECoG electrodes. The goal of this study was to investigate the effect of prior stimuli on the subsequent stimulus window. Specifically, the study was focused on two key parameters: dB differences and latency differences. Given the striking similarity between rat and human mechanoreceptors [13], investigating the response of rat hind paw mechanoreceptors to vibrotactile stimulation can directly inform and guide research in the development of neuroprosthetic devices for human application. Besides, the lack of information in the literature regarding the electrophysiological relevance of vibrotactile forward masking underscores the need for further research in this area. Furthermore, this research aims to address the limited number of studies focusing on this specific region in the existing literature; for instance, spike activity was investigated in the past [81]. While spike activity has been studied, investigating epidural field potentials recorded at the population level offers a unique perspective on amplitude and frequency encoding mechanisms in the context of forward masking. The utilization of surface electrodes for recording epidural field potentials presents some advantages, such as the mitigation of tissue reaction.

5.1 Overall Conclusion

In line with our initial hypothesis, the general trend indicates a suppressive effect of the prior stimulus on the test stimulus. This suppression was influenced by the frequency and amplitude of the test and prior stimulus, supporting our priori expectations. Moreover, our hypothesis that the suppression effect of the temporal proximity was also confirmed. The data showed that an increase in the temporal gap led to a decrease in the suppressive effect of the prior stimulus. This suggests that the suppressive influence of the prior stimulus is more pronounced when the test stimulus closely follows it. The maximum suppression was around 7 dB, suggesting that the

prior stimulus effectively suppressed the epidural field potential in the onset window, reducing it by approximately half.

The prior and test stimulus' frequency and amplitude of the test stimulus were also found to have statistically significant effects on the latency difference. As the frequency of the prior stimulus increased, the degree of delay also increased, reaching a maximum of 22 milliseconds, which could potentially signify more failures in synaptic transmission. This demonstrates the significant role of the prior stimulus in determining the subsequent response's timing and could be associated with variations in neurotransmitter levels influenced by the prior stimulus or alterations in receptor sensitivity in the somatosensory cortex.

5.2 Comparison with the Previous Literature

Our findings provide insights that can help elucidate the results of psychophysics studies on forward masking. In both the auditory and tactile domains, the relationship between the amount of masking and the amplitude of the masker is non-linear, yet it is directly proportional [82]. This means that as the amplitude of the masker increases, the degree of masking also increases. Specifically, we observed that an increase in the prior stimulus amplitude, a factor known to strengthen masking effects according to Gescheider's study [9], corresponded to suppression effects in the dB difference, as demonstrated by our results.

Furthermore, our study provides an electrophysiological basis to explain the inverse relationship observed in another study conducted by Gescheider between the amount of masking and the temporal gap between the masking and test stimulus [79]. Similarly, in the auditory domain, it has been consistently observed that the amount of forward masking is inversely proportional to the time interval between the mask and test stimuli [83]. In other words, the temporal gap between the two stimuli increases, the extent of forward masking decreases. We also observed the highest dB difference when the temporal gap was 100 msec, while the lowest dB difference was observed when

the temporal gap was 300 msec. These results suggest that the temporal proximity between the masking and test stimulus plays a critical role in modulating the extent of masking effects.

According to the literature, the spectral relationship between the masker and the signal can also impact the level of masking. It is generally expected that masking will be more pronounced when the masker and signal share the same frequency. Conversely, as the spectral differences between the masker and the signal increase, the degree of masking tends to decrease [84]. In the auditory domain, previous studies in forward and simultaneous masking have consistently shown higher levels of masking when the masker and the signal share the same frequency [83, 82]. However, our study presents a contrasting finding. We observed that when the prior stimulus and the test stimulus differed from each other, such as using a 250 Hz prior stimulus and a 5 Hz test stimulus, it resulted in greater suppression in terms of the dB difference. There could be two potential explanations for these contradictory observations. First, all stimuli used in the experiments were at the suprathreshold level. Consequently, the in-channel effect was not directly comparable because this stimulus level activates all channels. Second, former studies using spike recordings have demonstrated that a 5 Hz stimulus induces an entrainment pattern, while a 250 Hz stimulus lead to spikes mainly at the onset of the stimulus and a strong inhibition for the duration of the stimulus. Therefore, the observation that the 250 Hz prior stimulus leads to greater suppression than the 5 Hz prior stimulus can be attributed to the sustained inhibition caused by the 250 Hz prior stimulus[3].

Overall, these results suggest that the relationship between the frequency of the prior stimulus and the test stimulus and the resulting masking effects can be complex and dependent on specific experimental conditions.

5.3 Limitations and Future Work

This study aimed to elucidate the electrophysiological mechanisms underlying the forward masking paradigm observed in human psychophysics studies. By gaining a deeper understanding of the electrophysiological basis of the forward masking paradigm, there is potential for the development of more accurate and realistic simulations of tactile stimuli. However, it is important to acknowledge that this study has certain limitations.

While the psychophysical studies referenced earlier focus on human mechanisms, it is essential to note that this current study used rat models. The mechanisms underlying human-specific somatosensory processing may differ significantly. For instance, the rat hindlimb is characterized by a meager count of Pacinian receptors in that area [85], while the human hand hosts many of these receptors. This difference in receptor distribution could contribute to disparate sensory processing mechanisms between humans and rats.

Another limitation is the amplitude of the stimuli. All stimuli applied were at the suprathreshold level, which complicates the interpretation of the effects of spectral distance. Adjustments to the threshold level can only be accurately assessed using spike recordings and cannot be evaluated by recording epidural field potentials. Moreover, the time-averaging method utilized in this study has the potential to smooth out asynchronous signals, leading to a loss of spectral band energies. This smoothing effect might compromise the accuracy of the results, particularly concerning the representation of spectral complexities. The effect of gender on the dependent variables was also examined in our study, but no statistically significant effect was found (dB difference $p = 0.98$, latency difference $p = 0.71$).

In future investigations, exploring the effects of the duration of the prior stimulus could be insightful. There are already related studies within the field of human psychophysics that have explored the effects of the masker stimulus's duration. The analysis can be expanded in that respect. As discussed earlier, a time-frequency analy-

sis could provide more detailed information about the spectral bands of EFPs. Previous research has linked increased power in the gamma band with somatosensory processing related to this region [10]. Incorporating such an approach could offer a detailed understanding of the frequency-dependent characteristics of neural responses and potentially reveal important dynamics related to somatosensory processing. To enhance the analysis of important interactions between stimulus frequencies, incorporating coherence measurements would be beneficial. Coherence measurements provide valuable insights into the degree of synchronization and consistency between the frequencies. Furthermore, neurotransmitters play an important role in the processing of somatosensory information. Specifically, GABAergic and Glutamatergic effects can be examined in future studies [86]. It is important to note that this study was not designed to investigate gender effects. The gender effects can also be examined in future studies.

This study's results could improve the neuroprosthetic design, especially for devices that simulate touch sensation. By understanding the physiological underpinnings of the forward masking paradigm, the development of neuroprosthetics that offer more natural sensory feedback can be advanced.

REFERENCES

1. Kandel, E. R., J. H. Schwartz, and T. M. Jessell, eds., *Principles of Neural Science*, New York: Elsevier, third ed., 1991.

2. Güçlü, B., and S. J. Bolanowski, "Frequency responses of cat rapidly adapting mechanoreceptive fibers," *Somatosensory & Motor Research*, Vol. 20, pp. 249 – 263, 2003.

3. Vardar, B., and B. Güçlü, "Non-nmda receptor-mediated vibrotactile responses of neurons from the hindpaw representation in the rat si cortex," *Somatosensory Motor Research*, Vol. 34, pp. 189–203, 07 2017.

4. Schalk, G., and J. Mellinger, "Brain sensors and signals," 01 2010.

5. Schwartz, A. B., X. T. Cui, D. Weber, and D. W. Moran, "Brain-controlled interfaces: Movement restoration with neural prosthetics," *Neuron*, Vol. 52, no. 1, pp. 205–220, 2006.

6. Buzsáki, G., C. Anastassiou, and C. Koch, "The origin of extracellular fields and currentsâeeg, ecog, lfp and spikes," *Nature reviews. Neuroscience*, Vol. 13, pp. 407–20, 05 2012.

7. Simeral, J. D., S.-P. Kim, M. J. Black, J. P. Donoghue, and L. R. Hochberg, "Neural control of cursor trajectory and click by a human with tetraplegia 1000 days after implant of an intracortical microelectrode array," *Journal of Neural Engineering*, Vol. 8, p. 025027, mar 2011.

8. Musiek, F. E., and G. D. Chermak, "Chapter 18 - psychophysical and behavioral peripheral and central auditory tests," in *The Human Auditory System* (Aminoff, M. J., F. Boller, and D. F. Swaab, eds.), Vol. 129 of *Handbook of Clinical Neurology*, pp. 313–332, Elsevier, 2015.

9. Gescheider, G. A., K. E. Santoro, J. C. Makous, and S. J. Bolanowski, "Vibrotactile forward masking: Effects of the amplitude and duration of the masking stimulus," *The Journal of the Acoustical Society of America*, Vol. 98, pp. 3188–3194, 12 1995.

10. Duvan, T., "Functional characterization of graphene-based thin-film microelectrodes on rat," 2020.

11. Chapin, J. K., and C.-S. Lin, "Mapping the body representation in the si cortex of anesthetized and awake rats," *Journal of Comparative Neurology*, Vol. 229, no. 2, pp. 199–213, 1984.

12. Kalcheim, C., and N. M. Le Douarin, "Requirement of a neural tube signal for the differentiation of neural crest cells into dorsal root ganglia," *Developmental Biology*, Vol. 116, no. 2, pp. 451–466, 1986.

13. Leem, J. W., W. D. Willis, and J. M. Chung, "Cutaneous sensory receptors in the rat foot," *Journal of Neurophysiology*, Vol. 69, no. 5, pp. 1684–1699, 1993. PMID: 8509832.

14. Johansson, R., U. Landström, and R. Lundström, "Responses of mechanoreceptive afferent units in the glabrous skin of the human hand to sinusoida skin displacements," *Brain Research*, Vol. 244, pp. 17–25, 08 1982.

15. Johnson, K. O., "The roles and functions of cutaneous mechanoreceptors," *Current Opinion in Neurobiology*, Vol. 11, no. 4, pp. 455–461, 2001.

16. Brecht, M., B. Preilowski, and M. M. Merzenich, "Functional architecture of the mystacial vibrissae," *Behavioural Brain Research*, Vol. 84, no. 1, pp. 81–97, 1997.

17. "The tactile hair follicles in the mouse," *The Anatomical record*, Vol. 115, no. 2, p. 129â149, 1953.

18. "Responses of rat trigeminal ganglion neurons to movements of vibrissae in different directions," *Somatosensory Motor Research*, Vol. 7, no. 1, p. 47â65, 1990.

19. "Microelectrode delineation of fine grain somatotopic organization of (smi) cerebral neocortex in albino rat," *Brain Res*, Vol. 26, p. 259â275, 1971.

20. "Electromyographic activity of mystacial pad musculature during whisking behavior in the rat," *Somatosensory Motor Research*, Vol. 8, no. 2, pp. 159–64, 1991.

21. Cao, Y., S. Roy, R. N. S. Sachdev, and D. H. Heck, "Dynamic correlation between whisking and breathing rhythms in mice," *Journal of Neuroscience*, Vol. 32, no. 5, pp. 1653–1659, 2012.

22. Berg, R. W., and D. Kleinfeld, "Rhythmic whisking by rat: Retraction as well as protraction of the vibrissae is under active muscular control," *Journal of Neurophysiology*, Vol. 89, no. 1, pp. 104–117, 2003. PMID: 12522163.

23. Deschênes, M., J. Takatoh, A. Kurnikova, J. Moore, M. Demers, M. Elbaz, T. Furuta, F. Wang, and D. Kleinfeld, "Inhibition, not excitation, drives rhythmic whisking," *Neuron*, Vol. 90, no. 2, pp. 374–387, 2016.

24. Kim, U., and F. F. Ebner, "Barrels and septa: Separate circuits in rat barrel field cortex," *Journal of Comparative Neurology*, Vol. 408, no. 4, pp. 489–505, 1999.

25. Leiser, S. C., and K. A. Moxon, "Responses of trigeminal ganglion neurons during natural whisking behaviors in the awake rat," *Neuron*, Vol. 53, p. 117â133, January 2007.

26. Ferezou, I., S. Bolea, and C. C. Petersen, "Visualizing the cortical representation of whisker touch: Voltage-sensitive dye imaging in freely moving mice," *Neuron*, Vol. 50, no. 4, pp. 617–629, 2006.

27. Dombeck, D., A. Khabbaz, F. Collman, T. Adelman, and D. Tank, "Imaging large-scale neural activity with cellular resolution in awake, mobile mice," *Neuron*, Vol. 56, pp. 43–57, 10 2007.

28. Garion, L., U. Dubin, Y. Rubin, M. Khateb, Y. Schiller, R. Azouz, and J. Schiller, "Texture coarseness responsive neurons and their mapping in layer 2â3 of the rat barrel cortex in vivo," *eLife*, Vol. 3, p. e03405, sep 2014.

29. Knutsen, P. M., and E. Ahissar, "Orthogonal coding of object location," *Trends in Neurosciences*, Vol. 32, no. 2, pp. 101–109, 2009.

30. Sofroniew, N. J., and K. Svoboda, "Whisking," *Current Biology*, Vol. 25, no. 4, pp. R137–R140, 2015.

31. OConnor, D. H., L. Krubitzer, and S. Bensmaia, "Of mice and monkeys: Somatosensory processing in two prominent animal models," *Progress in Neurobiology*, Vol. 201, p. 102008, 2021.

32. Severson, K. S., D. Xu, M. Van de Loo, L. Bai, D. D. Ginty, and D. H. OâConnor, "Active touch and self-motion encoding by merkel cell-associated afferents," *Neuron*, Vol. 94, no. 3, pp. 666–676.e9, 2017.

33. Wallach, A., K. Bagdasarian, and E. Ahissar, "On-going computation of whisking phase by mechanoreceptors," *Nature Neuroscience*, Vol. 19, 01 2016.

34. Smith, J., and K. Alloway, "Rat whisker motor cortex is subdivided into sensory-input and motor-output areas," *Frontiers in Neural Circuits*, Vol. 7, 2013.

35. Okoro, S. U., R. U. Goz, B. W. Njeri, M. Harish, C. F. Ruff, S. E. Ross, C. R. Gerfen, and B. M. Hooks, "Organization of cortical and thalamic input to inhibitory neurons in mouse motor cortex," *bioRxiv*, 2021.

36. Tutunculer, B., G. Foffani, B. T. Himes, and K. A. Moxon, "Structure of the excitatory receptive fields of infragranular forelimb neurons in the rat primary somatosensory cortex responding to touch," *Cerebral Cortex*, Vol. 16, pp. 791–810, 08 2005.

37. Kunori, N., and I. Takashima, "High-order motor cortex in rats receives somatosensory inputs from the primary motor cortex via cortico-cortical pathways," *European Journal of Neuroscience*, Vol. 44, no. 11, pp. 2925–2934, 2016.

38. Kao, T., J. S. Shumsky, M. Murray, and K. A. Moxon, "Exercise induces cortical plasticity after neonatal spinal cord injury in the rat," *Journal of Neuroscience*, Vol. 29, no. 23, pp. 7549–7557, 2009.

39. Nandakumar, B., G. H. Blumenthal, F. P. Pauzin, and K. A. Moxon, "Hindlimb Somatosensory Information Influences Trunk Sensory and Motor Cortices to Support Trunk Stabilization," *Cerebral Cortex*, Vol. 31, pp. 5165–5187, 06 2021.

40. Berger, H., "Über das elektrenkephalogramm des menschen," *Archiv für Psychiatrie und Nervenkrankheiten*, Vol. 87, pp. 527–570, 1929.

41. Kirschfeld, K., "The physical basis of alpha waves in the electroencephalogram and the origin of the âberger effectâ," *Biological Cybernetics*, Vol. 92, pp. 177–85, 04 2005.

42. Walter, W. G., "The location of cerebral tumours by electro-encephalography," *The Lancet*, Vol. 228, no. 5893, pp. 305–308, 1936.

43. Jasper, H. H., J. Kershman, and A. Elvidge, "Electroencephalographic studies of injury to the head," *Archives of Neurology Psychiatry*, Vol. 44, pp. 328–350, 08 1940.

44. Schomer, D. L., F. H. Lopes da Silva, R. Sutter, P. W. Kaplan, and D. L. Schomer, "3C1Historical Aspects of Electroencephalography," in *Niedermeyer's Electroencephalography: Basic Principles, Clinical Applications, and Related Fields*, Oxford University Press, 11 2017.

45. Aserinsky, E., and N. Kleitman, "Regularly occurring periods of eye motility, and concomitant phenomena, during sleep," *Science*, Vol. 118, no. 3062, pp. 273–274, 1953.

46. Oddo, M., and A. Rossetti, "Early multimodal outcome prediction after cardiac arrest in patients treated with hypothermia," *Critical Care Medicine*, Vol. 42, 01 2014.

47. Başar-Eroğlu, C., and E. Başar, "A compound p300-40hz response of the cat hippocampus," *International Journal of Neuroscience*, Vol. 60, no. 3-4, pp. 227–237, 1991.

48. Li, Y., J. Long, T. Yu, Z. Yu, C. Wang, H. Zhang, and C. Guan, "An eeg-based bci system for 2-d cursor control by combining mu/beta rhythm and p300 potential," *IEEE Transactions on Biomedical Engineering*, Vol. 57, no. 10, pp. 2495–2505, 2010.

49. Seno, B., M. Matteucci, and L. Mainardi, "Online detection of p300 and error potentials in a bci speller," *Computational Intelligence and Neuroscience*, Vol. 2010, p. 307254, 01 2010.

50. Pfurtscheller, G., C. Brunner, A. Schlögl, and F. Lopes da Silva, "Mu rhythm (de)synchronization and eeg single-trial classification of different motor imagery tasks," *NeuroImage*, Vol. 31, no. 1, pp. 153–159, 2006.

51. Presacco, A., R. Goodman, L. Forrester, and J. L. Contreras-Vidal, "Neural decoding of treadmill walking from noninvasive electroencephalographic signals," *Journal of Neurophysiology*, Vol. 106, no. 4, pp. 1875–1887, 2011. PMID: 21768121.

52. Ortiz, M., L. Ferrero, E. Iáñez, J. M. Azorin, and J. L. Contreras-Vidal, "Sensory integration in human movement: A new brain-machine interface based on gamma band and attention level for controlling a lower-limb exoskeleton," *Frontiers in Bioengineering and Biotechnology*, Vol. 8, 2020.

53. Palmini, A., "The concept of the epileptogenic zone: A modern look at penfield and jasper's views on the role of interictal spikes," *Epileptic disorders : international epilepsy journal with videotape*, Vol. 8 Suppl 2, pp. S10–5, 08 2006.

54. "Somatosensory ecog-based brainâmachine interface with electrical stimulation on medial forebrain bundle," *Biomedical Engineering Letters*, Vol. 13, pp. 85–95, feb 2023.

55. Steinmetz, N. A., C. Koch, K. D. Harris, and M. Carandini, "Challenges and opportunities for large-scale electrophysiology with neuropixels probes," *Current Opinion in Neurobiology*, Vol. 50, pp. 92 – 100, 2018.

56. Trevelyan, A. J., "The direct relationship between inhibitory currents and local field potentials," *Journal of Neuroscience*, Vol. 29, no. 48, pp. 15299–15307, 2009.

57. Ray, S., and J. H. R. Maunsell, "Different origins of gamma rhythm and high-gamma activity in macaque visual cortex," *PLOS Biology*, Vol. 9, pp. 1–15, 04 2011.

58. Rickert, J., S. C. de Oliveira, E. Vaadia, A. Aertsen, S. Rotter, and C. Mehring, "Encoding of movement direction in different frequency ranges of motor cortical local field potentials," *Journal of Neuroscience*, Vol. 25, no. 39, pp. 8815–8824, 2005.

59. Adrian, E. D., and Y. Zotterman, "The impulses produced by sensory nerve-endings," *The Journal of Physiology*, Vol. 61, no. 2, pp. 151–171, 1926.

60. Hodgkin, A. L., and A. F. Huxley, "A quantitative description of membrane current and its application to conduction and excitation in nerve," *The Journal of Physiology*, Vol. 117, no. 4, pp. 500–544, 1952.

61. Strumwasser, F., "Long-term recording from single neurons in brain of unrestrained mammals," *Science*, Vol. 127, no. 3296, pp. 469–470, 1958.

62. Nicolelis, M., "Actions from thoughts," *Nature*, Vol. 409, pp. 403–7, 02 2001.

63. Burt, C., "Gustav theodor fechner elemente der psychophysik 1860," *British Journal of Statistical Psychology*, Vol. 13, no. 1, pp. 1–10, 1960.

64. Güçlü, B., and S. J. Bolanowski, "Vibrotactile thresholds of the non-pacinian i channel: I. methodological issues," *Somatosensory & Motor Research*, Vol. 22, no. 1-2, pp. 49–56, 2005. PMID: 16191758.

65. Güçlü, B., C. Tanidir, N. Mukaddes, and F. Unal, "Tactile sensitivity of normal and autistic children," *Somatosensory Motor research*, Vol. 24, pp. 21–33, 07 2009.

66. Güçlü, B., and Çiğdem Öztek, "Tactile sensitivity of children: Effects of frequency, masking, and the non-pacinian i psychophysical channel," *Journal of Experimental Child Psychology*, Vol. 98, no. 2, pp. 113–130, 2007.

67. Güçlü, B., "Deviation from weber's law in the non-pacinian i tactile channel: A psychophysical and simulation study of intensity discrimination," *Neural Computation*, Vol. 19, no. 10, pp. 2638–2664, 2007.

68. Güçlü, B., E. Sevinc, and R. Canbeyli, "Duration discrimination by musicians and nonmusicians," *Psychological Reports*, Vol. 108, no. 3, pp. 675–687, 2011. PMID: 21879613.

69. Muniak, M., S. Ray, S. Hsiao, J. Dammann, and S. Bensmaia, "The neural coding of stimulus intensity: Linking the population response of mechanoreceptive afferents with psychophysical behavior," *The Journal of neuroscience : the official journal of the Society for Neuroscience*, Vol. 27, pp. 11687–99, 11 2007.

70. Güçlü, B., and S. Dinçer, "Neural coding in the non-pacinian i tactile channel: A psychophysical and simulation study of magnitude estimation," *Somatosensory motor research*, Vol. 30, 11 2012.

71. Greenspan, J. D., and S. J. Bolanowski, "Chapter 2 - the psychophysics of tactile perception and its peripheral physiological basis," in *Pain and Touch* (Kruger, L., ed.), Handbook of Perception and Cognition, pp. 25–103, San Diego: Academic Press, 1996.

72. Bolanowski, S., G. Gescheider, R. Verrillo, and C. Checkosky, "Four channels mediate the mechanical aspects of touch," *The Journal of the Acoustical Society of America*, Vol. 84, pp. 1680–94, 12 1988.

73. Francis, G., *Masking*. John Wiley Sons, Ltd, 2006.

74. Purves, D., D. Fitzpatrick, L. Katz, A. Lamantia, J. McNamara, S. Williams, and G. Augustine, *Neuroscience*, Sinauer Associates, 2000.

75. Enns, J., and V. Di Lollo, "What's new in visual masking?," *Trends in Cognitive Sciences*, Vol. 4, pp. 345–352, 09 2000.

76. Blake, R., "Vision: visual masking. an integrative approach. bruno g. breitmeyer. clarendon (oxford university press), new. york, 1984. x, 454 pp., illus. $34.95. oxford psychology series no. 4.," *Science*, Vol. 228, no. 4701, pp. 864–865, 1985.

77. Bridgeman, B., "Visual evoked potentials: Concomitants of metacontrast in late components," *Perception Psychophysics*, Vol. 43, pp. 401–403, 07 1988.

78. Gescheider, G., J. Wright, and R. Verrillo, "Information-processing channels in the tactile sensory system: A psychophysical and physiological analysis," *Information-Processing Channels in the Tactile Sensory System: A Psychophysical and Physiological Analysis*, pp. 1–135, 01 2008.

79. Gescheider, G. A., and N. Migel, "Some temporal parameters in vibrotactile forward masking," *The Journal of the Acoustical Society of America*, Vol. 98, pp. 3195–3199, 12 1995.

80. Peirce, B., "On peirce's criterion," *Proceedings of the American Academy of Arts and Sciences*, Vol. 13, pp. 348–351, 1877.

81. İsmail Devecioğlu, and B. Güçlü, "A novel vibrotactile system for stimulating the glabrous skin of awake freely behaving rats during operant conditioning," *Journal of Neuroscience Methods*, Vol. 242, pp. 41–51, 2015.

82. Gelfand, S., *Hearing: An Introduction to Psychological and Physiological Acoustics*, Elsevier Science, 2013.

83. Moore, B. C. J., and S. M. A. Ernst, "Frequency difference limens at high frequencies: Evidence for a transition from a temporal to a place code," *The Journal of the Acoustical Society of America*, Vol. 132, pp. 1542–1547, 09 2012.

84. Viemeister, N. F., and C. J. Plack, *Time Analysis*, pp. 116–154. New York, NY: Springer New York, 1993.

85. Walcher, J., J. Ojeda-Alonso, J. Haseleu, M. K. Oosthuizen, A. H. Rowe, N. C. Bennett, and G. R. Lewin, "Specialized mechanoreceptor systems in rodent glabrous skin," *The Journal of Physiology*, Vol. 596, no. 20, pp. 4995–5016, 2018.

86. Lee, S., I. Kruglikov, J. Huang, G. Fishell, and B. Rudy, "A disinhibitory circuit mediates motor integration in the somatosensory cortex," *Nature Neuroscience*, Vol. 16, 10 2013.